Wave Motion 51 (2014) 967–985

Contents lists available at ScienceDirect

Wave Motion

journal homepage: www.elsevier.com/locate/wavemoti

Phase velocity effects of the wave interaction with exponentially sheared current

Zeng Liu [a], Zhiliang Lin [a], Shijun Liao [a,b,c,*]

[a] State Key Laboratory of Ocean Engineering, Shanghai 200240, China

[b] School of Naval Architecture, Ocean and Civil Engineering, Shanghai Jiaotong University, Shanghai 200240, China

[c] Nonlinear Analysis and Applied Mathematics Research Group (NAAM), King Abdulaziz University (KAU), Jeddah, Saudi Arabia

HIGHLIGHTS

- The influence of the rotational current on the unidirectional bichromatic wave-train is studied.
- A model without small physical parameters.
- High-order approximation solutions.

ARTICLE INFO

Article history:
Received 13 August 2013
Received in revised form 21 February 2014
Accepted 30 March 2014
Available online 5 April 2014

Keywords:
Phase velocity
Nonlinear wave–current interaction
Vorticity

ABSTRACT

The nonlinear interaction between the unidirectional bichromatic wave-train and exponentially sheared current in water of an infinite depth is investigated. The model is based on the vorticity transport equation and the exact free surface conditions, without any assumptions for the existence of small physical parameters. Earlier works of the wave–current interaction were mainly restricted to either current acted on the monochromatic wave or irregular waves limited to irrotational current. Different from these previous works, no constraint is made in our model for amplitudes of the primary wave, and the current owns an exponential type profile along the vertical line. To ensure that the effect of vorticity on the phase velocity is consistent with earlier derivation, the case of a small amplitude wave traveling on the exponentially sheared current is examined firstly. Then the effect of nonlinearity on the phase velocity of primary waves in a bichromatic wave-train is considered. Accurate high-order approximations of the phase velocity are obtained under consideration of both the nonlinear wave self–self and mutual interactions. Finally, the combined effect of vorticity and nonlinearity on the phase velocity is investigated through the case of a bichromatic wave-train propagating on an exponentially sheared current. It is found that the characteristic current slope determines the effect of vorticity on the phase velocity caused by nonlinear wave self–self and mutual interactions, and the surface current strength may amplify/reduce this effect.

1. Introduction

Searching solutions for the wave–current interaction has arisen interests of a lot of researchers. Early works were mainly focused on uniform current and constant vorticity for linear waves [1–3] and nonlinear waves [4,5].

* Corresponding author at: School of Naval Architecture, Ocean and Civil Engineering, Shanghai Jiaotong University, Shanghai 200240, China.
E-mail address: sjliao@sjtu.edu.cn (S. Liao).

http://dx.doi.org/10.1016/j.wavemoti.2014.03.009
0165-2125/

For linear waves riding on an arbitrary weak current, the first attempt for the current decaying exponentially with depth is considered by Abdullah [6]. Based on the work of [7], the dispersion relation for the depth-dependent current is examined by Skop [8,9], then later Kirby and Chen [10] extended it to the second order. The prediction of wavelength and particle velocities is considered by Thomas [11] after compared the linear theory with a parallel experiment.

For nonlinear regular waves co-existing with an arbitrary current, there are generally two methods. One is to approximate the current profile by a number of straight line elements [12,13], while the other is to convert the original domain to a rectangular one through Dubreil–Jacotin transformation [14–17]. Besides, Swan and James [18] presented a second-order perturbation analysis for small amplitude waves. And through experimental results, Thomas [15] demonstrated the importance of the global vorticity distribution in the wave–current interaction and Swan et al. [19] confirmed that the near-surface vorticity leads to an important modification of the dispersion equation. For more details about the early works, please refer to the monographs [20–23].

Compared with the huge literature concerning monochromatic waves, the investigation of the current acted on irregular waves is considerably less developed, owing to its complexity. Experiments were performed by, e.g. Simons and MacIver [24], who measured the mean, wave-induced and turbulent velocities, instantaneous bed shear stresses, wavelengths and wave heights for regular, bichromatic and random waves propagating with and against a turbulent current, as well as by Umeyama [25], whose experimental data suggested that the wave direction is an important factor to change the vertical profile of the mean velocity based on the logarithmic law. In theory, Chen et al. [26] developed the Boussinesq-type equations explicitly incorporating the depth-uniform current on near-resonant triad interactions of waves in shallow water, while Madsen and Fuhrman [27,28] incorporate the effect of an ambient current with the option of specifying zero net volume flux on their third-order perturbation solutions for multi-directional irregular water waves in finite depth based on the potential function. A novel numerical method has been developed by Nwogu [29] to investigate the modulational instability of deep-water waves riding on both depth-uniform and exponentially sheared current.

The phase velocity is a topic that received the greatest attention in the literature in the field of wave–current interactions. Following the pioneering work of Longuet-Higgins and Phillips [30] considering the change in phase velocity due to the mutual interaction between different primary waves, Hogan et al. [31] extended their solution to cover gravity–capillary waves in deep water, Zhang and Chen [32] extended the interactions to three collinear deep-water wave components, Tanaka et al. [33] extended it to the interaction among component waves in a continuous energy spectrum, and Madsen and Fuhrman [27,28] provided a new third-order finite-depth formulation for the mutual interaction. However, all of the published formulas are the third-order approximations, which are suitable only for the small-amplitude wave interaction. As the amplitudes of primary waves increase, high-order approximations are required. Besides, the influence of vorticity on the mutual interaction between different primary waves has been nearly ignored since [30]. When vorticity appears in the ambient current, how the phase velocity of each primary wave is modified by the presence of the other is still an open problem.

In this article, a nonlinear model of the unidirectional bichromatic wave-train riding on the current with variable distribution of vorticity is considered. Different from approaches mentioned above, no constraint is made for the primary wave amplitudes, and following Abdullah [6], a current that decays exponentially with depth is studied. A high-order approximation of the phase velocity concerning both nonlinear wave self–self and mutual interactions is derived, which provides accurate solutions for finite-amplitude wave interactions. In addition, the effect of vorticity from the ambient current on the phase velocity caused by the nonlinear wave mutual interaction is investigated in detail.

The present paper is organized as follows. Section 2 illustrates the mathematical model, which is an extension of [10] for finite-amplitude waves. In Section 3, a brief description of the analytic procedure based on the homotopy analysis method (hereinafter, HAM) [34,35] is described. The phase velocity of linear waves propagating on current and nonlinear wave interactions with/without current are considered in Section 4. Finally, the concluding remarks are given in Section 5, with some deductions provided in the Appendix.

2. Mathematical model

Choose Cartesian coordinates (x, y) as the x-axis being the direction of wave propagation and y measured vertically upwards, with the origin located on the mean water level as shown in Fig. 1. The current is assumed uniform in the horizontal but owns a vertically exponential distribution of velocity. The free-surface elevation is denoted by $\zeta(x, t)$. The fluid is assumed to be inviscid and incompressible, so that we can introduce the stream function $\psi(x, y, t)$ defined by $\psi_y(x, y, t) = u(x, y, t)$, $\psi_x(x, y, t) = -v(x, y, t)$. The problem is governed by the vorticity transport equation

$$\psi_{xxt} + \psi_{yyt} + \psi_y(\psi_{xxx} + \psi_{xyy}) - \psi_x(\psi_{xxy} + \psi_{yyy}) = 0. \tag{1}$$

In the infinite water depth, we have the bed condition

$$\psi_x \to 0, \quad \text{as } y \to -\infty. \tag{2}$$

On the free surface $\zeta(x, t)$, we have the kinematic and dynamic free-surface conditions

$$\zeta_x\psi_y + \psi_x + \zeta_t = 0, \quad \text{on } y = \zeta(x, t), \tag{3}$$

$$P(x, y, t) - P_0 = 0, \quad \text{on } y = \zeta(x, t), \tag{4}$$

where $P(x, y, t)$ denotes the pressure of the field and P_0 is the constant atmospheric pressure.

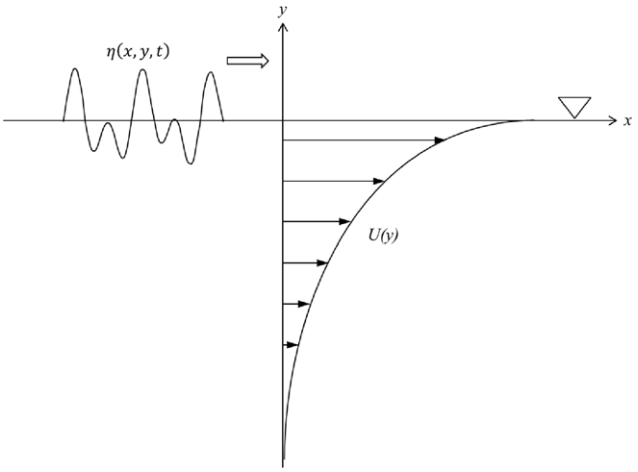

Fig. 1. Definition sketch.

For irregular waves or even the simplest bichromatic wave-train, no steady solution exists in any coordinates due to the complex behavior of the wave interaction: the free surface is no longer a streamline so that the Dubreil–Jacotin transformation applied by [14–17] is not valid any more. Furthermore, the exponentially sheared current imposes a vorticity over the whole fluid field. The subsequent wave motion thereby inherits a rotational motion, so that the traditional Bernoulli's equation based on the velocity potential is therefore inadequate [6].

In order to constitute a closure model for the stream function and the elevation, we make use of the chain rule of differentiation [36]:

$$P_y\zeta_t + P_t = 0, \tag{5}$$

$$P_y\zeta_x + P_x = 0. \tag{6}$$

Such a way of recasting the dynamic free-surface boundary condition is proposed by McDonald and Witting [36] and has recently been extended by Nwogu [29]. Substituting the pressure gradients from the Euler equations

$$\frac{\partial^2\psi}{\partial y\partial t} + \frac{\partial\psi}{\partial y}\frac{\partial^2\psi}{\partial x\partial y} - \frac{\partial\psi}{\partial x}\frac{\partial^2\psi}{\partial y^2} = -\frac{1}{\rho}\frac{\partial P}{\partial x}, \tag{7}$$

$$-\frac{\partial^2\psi}{\partial x\partial t} - \frac{\partial\psi}{\partial y}\frac{\partial^2\psi}{\partial x^2} + \frac{\partial\psi}{\partial x}\frac{\partial^2\psi}{\partial x\partial y} + g = -\frac{1}{\rho}\frac{\partial P}{\partial y}, \tag{8}$$

into (6), we obtain the x momentum equation in terms of the tangential fluid acceleration at the free-surface $\zeta(x, t)$:

$$\frac{\partial^2\psi}{\partial y\partial t} + \frac{\partial\psi}{\partial y}\frac{\partial^2\psi}{\partial x\partial y} - \frac{\partial\psi}{\partial x}\frac{\partial^2\psi}{\partial y^2} - \left(\frac{\partial^2\psi}{\partial x\partial t} + \frac{\partial\psi}{\partial y}\frac{\partial^2\psi}{\partial x^2} - \frac{\partial\psi}{\partial x}\frac{\partial^2\psi}{\partial x\partial y} - g\right)\frac{\partial\zeta}{\partial x} = 0. \tag{9}$$

The nonlinear partial differential equation (1), subject to the bed condition (2) and two nonlinear free-surface conditions (3) and (9), constitute a closure model for the stream function and the elevation. This model can be simplified into the model studied by Kirby and Chen [10] for the linear wave and is valid for multiple waves with finite amplitudes, thus is more general.

3. Solution procedure

For simplicity, we consider the steady-state situation of the problem, i.e. the amplitudes of all wave components are constants. In other words, the spectrum of wave energy is independent of the time t. Besides, without loss of generality, let us consider the interaction of two finite-amplitude unidirectional progressive periodic waves.

3.1. Solution expression of the stream function without current

For unidirectional bichromatic waves, it is convenient to introduce the transformation

$$\xi_1 = k_1x - k_1c_1t, \qquad \xi_2 = k_2\,x - k_2\,c_2\,t, \tag{10}$$

where k_1, k_2 denote wave numbers, and c_1, c_2 are the phase speeds of two primary wave components, respectively. Here c_1 and c_2 are unknown, which will be determined later.

As all the amplitudes of wave components are assumed to be constant, the wave elevation $\zeta(\xi_1, \xi_2)$ can be expressed by

$$\zeta(\xi_1, \xi_2) = \sum_{i=0}^{+\infty} \sum_{j=-\infty}^{+\infty} C_{i,j}^{\zeta} \cos(i\xi_1 + j\xi_2), \tag{11}$$

where $C_{i,j}^{\zeta}$ is a constant to be determined. For the fluid field without current, no vorticity exists so that

$$\Omega = -\psi_{xx} - \psi_{yy} = k_1^2 \frac{\partial^2 \psi}{\partial \xi_1{}^2} + 2k_1 k_2 \frac{\partial^2 \psi}{\partial \xi_1 \partial \xi_2} + k_2^2 \frac{\partial^2 \psi}{\partial \xi_2{}^2} + \frac{\partial^2 \psi}{\partial y^2} \equiv 0. \tag{12}$$

Eq. (12) has the general solution

$$A \cos(m\xi_1 + n\xi_2) \ \exp\left[|mk_1 + nk_2|y\right], \tag{13}$$

where A is a constant and m, n are integers. Thus the irrotational stream function $\psi(\xi_1, \xi_2, y)$ can be expressed by

$$\psi(\xi_1, \xi_2, y) = \sum_{i=0}^{+\infty} \sum_{j=-\infty}^{+\infty} C_{i,j}^{\psi} \cos(i\xi_1 + j\xi_2) \exp[|ik_1 + jk_2|y], \tag{14}$$

where $C_{i,j}^{\psi}$ is a constant to be determined.

3.2. Solution expression of the stream function with current

When current with vorticity is added into the fluid field, the expression of surface elevation is the same as the case without current, only with a different value of $C_{i,j}^{\zeta}$ in (11). While the expression of surface elevation is very clear from the physical view-point, the expression of the stream function ψ is not so straightforward.

To derive the expression for stream function $\psi(\xi_1, \xi_2, y)$, we firstly rewrite the governing equation (1) in the new coordinates (ξ_1, ξ_2, y)

$$\begin{aligned}
&k_1^3 c_1 \frac{\partial^3 \psi}{\partial \xi_1^3} + k_1^2 k_2 (2c_1 + c_2) \frac{\partial^3 \psi}{\partial \xi_1^2 \xi_2} + k_1 k_2^2 (2c_2 + c_1) \frac{\partial^3 \psi}{\partial \xi_1 \xi_2^2} + k_2^3 c_2 \frac{\partial^3 \psi}{\partial \xi_2^3} \\
&\quad + k_1 c_1 \frac{\partial^3 \psi}{\partial \xi_1 \partial y^2} + k_2 c_2 \frac{\partial^3 \psi}{\partial \xi_2 \partial y^2} - \frac{\partial \psi}{\partial y} \left(k_1^3 \frac{\partial^3 \psi}{\partial \xi_1^3} + 3k_1^2 k_2 \frac{\partial^3 \psi}{\partial \xi_1^2 \xi_2} + 3k_1 k_2^2 \frac{\partial^3 \psi}{\partial \xi_1 \xi_2^2} \right. \\
&\quad \left. + k_2^3 \frac{\partial^3 \psi}{\partial \xi_2^3} + k_1 \frac{\partial^3 \psi}{\partial \xi_1 \partial y^2} + k_2 \frac{\partial^3 \psi}{\partial \xi_2 \partial y^2} \right) + \left(k_1 \frac{\partial \psi}{\partial \xi_1} + k_2 \frac{\partial \psi}{\partial \xi_2} \right) \\
&\quad \times \left(k_1^2 \frac{\partial^3 \psi}{\partial \xi_1^2 \partial y} + 2k_1 k_2 \frac{\partial^3 \psi}{\partial \xi_1 \partial \xi_2 \partial y} + k_2^2 \frac{\partial^3 \psi}{\partial \xi_2^2 \partial y} + \frac{\partial^3 \psi}{\partial y^3} \right) \\
&= \mathcal{N}_g[\psi(\xi_1, \xi_2, y), c_1, c_2] \\
&= \mathcal{L}_g[\psi(\xi_1, \xi_2, y), c_1, c_2] + \mathcal{M}_g[\psi(\xi_1, \xi_2, y), c_1, c_2] = 0.
\end{aligned} \tag{15}$$

The boundary conditions (3) and (9) on the free surface $y = \zeta(\xi_1, \xi_2)$ then become

$$\begin{aligned}
&k_1 c_1 \frac{\partial \zeta}{\partial \xi_1} + k_2 c_2 \frac{\partial \zeta}{\partial \xi_2} - \frac{\partial \psi}{\partial y} \left(k_1 \frac{\partial \zeta}{\partial \xi_1} + k_2 \frac{\partial \zeta}{\partial \xi_2} \right) - k_1 \frac{\partial \psi}{\partial \xi_1} - k_2 \frac{\partial \psi}{\partial \xi_2} = \mathcal{N}_{b,1}[\zeta(\xi_1, \xi_2), \psi(\xi_1, \xi_2, y), c_1, c_2] \\
&= \mathcal{L}_{b,1}[\zeta(\xi_1, \xi_2), \psi(\xi_1, \xi_2, y), c_1, c_2] + \mathcal{M}_{b,1}[\zeta(\xi_1, \xi_2), \psi(\xi_1, \xi_2, y), c_1, c_2] = 0,
\end{aligned} \tag{16}$$

$$\begin{aligned}
&k_1 c_1 \frac{\partial^2 \psi}{\partial \xi_1 \partial y} + k_2 c_2 \frac{\partial^2 \psi}{\partial \xi_2 \partial y} - \frac{\partial \psi}{\partial y} \left(k_1 \frac{\partial^2 \psi}{\partial \xi_1 \partial y} + k_2 \frac{\partial^2 \psi}{\partial \xi_2 \partial y} \right) + \left(k_1 \frac{\partial \psi}{\partial \xi_1} + k_2 \frac{\partial \psi}{\partial \xi_2} \right) \frac{\partial^2 \psi}{\partial y^2} \\
&\quad - \left\{ k_1^2 c_1 \frac{\partial^2 \psi}{\partial \xi_1{}^2} + (c_1 + c_2) k_1 k_2 \frac{\partial^2 \psi}{\partial \xi_1 \partial \xi_2} + k_2^2 c_2 \frac{\partial^2 \psi}{\partial \xi_2{}^2} - \frac{\partial \psi}{\partial y} \left(k_1^2 \frac{\partial^2 \psi}{\partial \xi_1{}^2} + 2k_1 k_2 \frac{\partial^2 \psi}{\partial \xi_1 \partial \xi_2} \right. \right. \\
&\quad \left. \left. + k_2^2 \frac{\partial^2 \psi}{\partial \xi_2{}^2} \right) + \left(k_1 \frac{\partial \psi}{\partial \xi_1} + k_2 \frac{\partial \psi}{\partial \xi_2} \right) \left(k_1 \frac{\partial^2 \psi}{\partial \xi_1 \partial y} + k_2 \frac{\partial^2 \psi}{\partial \xi_2 \partial y} \right) + g \right\} \left(k_1 \frac{\partial \zeta}{\partial \xi_1} + k_2 \frac{\partial \zeta}{\partial \xi_2} \right) \\
&= \mathcal{N}_{b,2}[\zeta(\xi_1, \xi_2), \psi(\xi_1, \xi_2, y), c_1, c_2] \\
&= \mathcal{L}_{b,2}[\zeta(\xi_1, \xi_2), \psi(\xi_1, \xi_2, y), c_1, c_2] + \mathcal{M}_{b,2}[\zeta(\xi_1, \xi_2), \psi(\xi_1, \xi_2, y), c_1, c_2] = 0,
\end{aligned} \tag{17}$$

and the bed condition (2) reads

$$\frac{\partial \psi}{\partial \xi_1} \to 0 \quad \text{and} \quad \frac{\partial \psi}{\partial \xi_2} \to 0, \quad \text{as } y \to -\infty, \tag{18}$$

where $\mathcal{N}_g$, $\mathcal{N}_{b,1}$ and $\mathcal{N}_{b,2}$ are the nonlinear operators, $\mathcal{L}_g$, $\mathcal{L}_{b,1}$ and $\mathcal{L}_{b,2}$ ($\mathcal{M}_g$, $\mathcal{M}_{b,1}$ and $\mathcal{M}_{b,2}$) denote the linear (remaining nonlinear) parts of the full operator, respectively.

It is known through the work of Ekman [37] that the surface oceanic current follows, approximately, a spiral law [6]. Following Abdullah [6] that focused on the magnitude of the current speed distribution, we consider the exponentially sheared current

$$U(y) = U_0 \exp[y/d], \quad -\infty < y \le \zeta(\xi_1, \xi_2), \tag{19}$$

where U_0 is the surface velocity of the current and d is the characteristic current depth. Here the ambient current is defined up to the instantaneous free-surface elevation [29]. As a first step, no feedback has been considered to the exponential current field, though the current profile could change as noticed by Swan et al. [19] and Nwogu [29].

Physically speaking, as the unidirectional irregular wave is periodic along the x direction and both the irregular waves and current decay exponentially along the y direction, it is reasonable to predict that the combined wave–current field still owns the periodicity in the x axis and decays exponentially in the y axis. Besides, the exponentially sheared current imposes a vorticity distribution, the subsequent wave motion thereby inherits a rotational motion [6].

Mathematically, to seek the detailed solution expression of $\psi(\xi_1, \xi_2, y)$, we substitute linear expression[1]

$$\psi(\xi_1, \xi_2, y) \sim \cos(i\xi_1 + j\xi_2) \exp[|ik_1 + jk_2|y] + \exp[y/d], \tag{20}$$

into the vorticity transport equation (15). From the first nonlinear term of (15), we find

$$\begin{aligned} \frac{\partial \psi}{\partial y}\frac{\partial^3 \psi}{\partial \xi_1^3} &\sim (\cos(i\xi_1 + j\xi_2) \exp[|ik_1 + jk_2|y] + \exp[y/d]) \sin(i'\xi_1 + j'\xi_2) \exp[|i'k_1 + j'k_2|y] \\ &\sim (\sin((i+i')\xi_1 + (j+j')\xi_2) - \sin((i-i')\xi_1 + (j-j')\xi_2)) \exp[(|ik_1 + jk_2| \\ &\quad + |i'k_1 + j'k_2|)y] + \sin(i'\xi_1 + j'\xi_2) \exp[(|i'k_1 + j'k_2| + 1/d)y]. \end{aligned} \tag{21}$$

Different form the irrotational expression (14), the vorticity of the above two terms is not equal to zero, which means that they belong to the rotational components. The appearance of these two terms demonstrates the influence of the exponential distribution of vorticity on the irrotational waves. Based on (20) and (21), we express $\psi(\xi_1, \xi_2, y)$ in the general form:

$$\psi(\xi_1, \xi_2, y) = U_0\, d \exp(y/d) + \sum_{i=0}^{+\infty} \sum_{j=-\infty}^{+\infty} \sum_{r=0}^{+\infty} \sum_{s=-\infty}^{+\infty} \sum_{l=0}^{+\infty} C^{\psi}_{i,j,r,s,l} \cos(i\xi_1 + j\xi_2) \exp[(|rk_1 + sk_2| + l/d)y], \tag{22}$$

where $C^{\psi}_{i,j,r,s,l}$ is a constant. For given $C^{\psi}_{1,0,1,0,0}$, $C^{\psi}_{0,1,0,1,0}$, $C^{\psi}_{0,0,0,0,1}$, all other constants $C^{\zeta}_{i,j}$ in (11) and $C^{\psi}_{i,j,r,s,l}$ in (22) will be determined by solving Eqs. (15)–(18). Note that (22) contains (14) as a special case and automatically satisfies the bed condition (18). Mathematically, the nonlinear PDEs (15)–(18) are rather difficult to solve, since the unknown stream function ψ is governed by the complicated nonlinear PDE (15), subject to two complicated nonlinear boundary conditions (16) and (17) on the unknown free-surface ζ, and in addition the two unknown phase speeds c_1 and c_2 need to determined. Details of the deformation equations together with the solution procedure in the frame of HAM are shown in the Appendix.

3.3. Result verification

Set

$$C^{\psi}_{1,0,1,0,0} = H_1\sqrt{g/k_1^3}, \qquad C^{\psi}_{0,1,0,1,0} = H_2\sqrt{g/k_2^3},$$

where H_1 and H_2 denote the dimensionless stream function amplitude of each primary wave, respectively. For a single traveling wave, the values of dimensionless stream function amplitude H and the traditional dimensionless amplitude ak are shown in Table 1. It can be found from Table 1 that $H < ak$ all the time and the value of $ak - H$ is much smaller as compared to the individual value of H and ak, especially for $H < 0.20$.

According to the dependence of the phase velocity on the primary wave amplitude, we divide c_j, the phase velocity[2] of the jth ($j = 1, 2$) primary wave, into three parts

$$c_1 = c_1^L(\varepsilon, \delta) + c_1^S(\varepsilon, \delta, H_1) + c_1^I(\varepsilon, \delta, \kappa, H_1, H_2), \tag{23}$$

$$c_2 = c_2^L(\varepsilon, \delta, \kappa) + c_2^S(\varepsilon, \delta, \kappa, H_2) + c_2^I(\varepsilon, \delta, \kappa, H_1, H_2), \tag{24}$$

where $\varepsilon = U_0/\sqrt{g/k_1}$ is the dimensionless velocity of the current on the surface, $\delta = 1/(k_1 d)$ the dimensionless characteristic current slope, and $\kappa = k_2/k_1$ the ratio of primary wave numbers, respectively. The first and second terms c_j^L and c_j^S denote the linear and self–self interaction parts of the jth primary wave, respectively, as observed in the solution for a single Stokes wave traveling on exponentially sheared current. The third term c_j^I is related to the mutual interactions between different primary waves on exponentially sheared current.

[1] Here the trivial coefficients have been ignored.

[2] Here, c_j is divided by $\sqrt{g/k_j}$ to gain a dimensionless form.

Table 1
The value of H and ak for the case of the single traveling wave.

H	0.05000	0.10000	0.15000	0.20000	0.25000	0.30000
ak	0.05002	0.10002	0.15047	0.20491	0.26108	0.32424

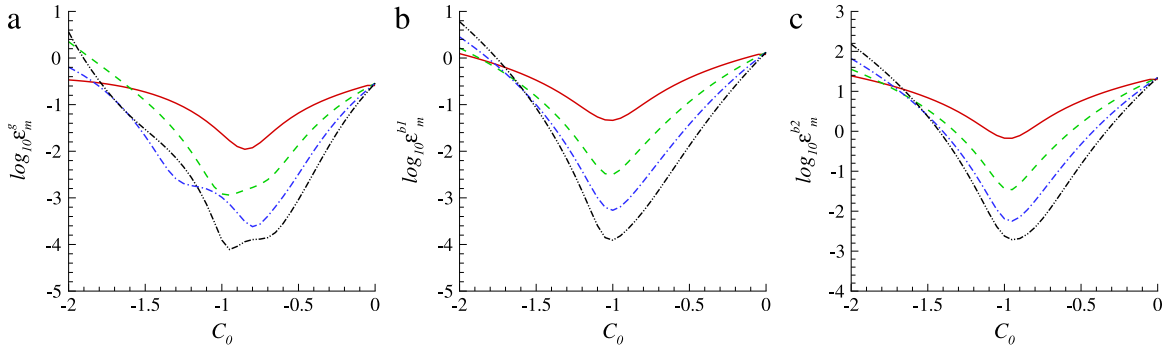

Fig. 2. (Color online) $\log_{10}\varepsilon_m^g$, $\log_{10}\varepsilon_m^{b,1}$ and $\log_{10}\varepsilon_m^{b,2}$ versus the convergence-control parameter C_0 with $H_1 = H_2 = 0.1$, $\varepsilon = 0.05$, $\delta = 4$ and $\kappa = 2\pi/3$. Solid line: 2nd-order approximation; Dashed line: 3rd-order approximation; Dash–dot line: 4th-order approximation; Dash–dot–dot line: 5th-order approximation.

HAM contains the so-called convergence-control parameter C_0 which provides us a convenient way to control and guarantee the convergence of approximation series [38,39]. This is a remarkable advantage of the HAM. For more examples, please refer to Liao's two books [34,35].

To determine the optimal value of C_0, we define the average residual squares of the vorticity transform equation (15) ε_m^g and the two free surface boundary conditions (16)–(17) $\varepsilon_m^{b,1}$ and $\varepsilon_m^{b,2}$:

$$\varepsilon_m^g = \frac{\pi^2}{100}\sum_{m=0}^{10}\sum_{n=0}^{10}\int_{-\infty}^{\zeta_m\left(\frac{\pi}{10}m,\,\frac{\pi}{10}n\right)}\left[\sum_{i=0}^{m-1}\Delta_i^g\left(\frac{\pi}{10}m,\,\frac{\pi}{10}n,\,y\right)\right]^2 dy \tag{25}$$

$$\varepsilon_m^{b,1} = \frac{\pi^2}{100}\sum_{m=0}^{10}\sum_{n=0}^{10}\left[\sum_{i=0}^{m-1}\Delta_i^{b,1}\left(\frac{\pi}{10}m,\,\frac{\pi}{10}n\right)\right]^2, \tag{26}$$

$$\varepsilon_m^{b,2} = \frac{\pi^2}{100}\sum_{m=0}^{10}\sum_{n=0}^{10}\left[\sum_{i=0}^{m-1}\Delta_i^{b,2}\left(\frac{\pi}{10}m,\,\frac{\pi}{10}n\right)\right]^2, \tag{27}$$

where Δ_i^g, $\Delta_i^{b,1}$ and $\Delta_i^{b,2}$ are the ith-order derivatives of $\mathcal{N}_b$, $\mathcal{N}_{b,1}$ and $\mathcal{N}_{b,2}$ with respect to q that defined by (B.4), (B.27) and (B.28), respectively.

In the case of $H_1 = H_2 = 0.1$, $\varepsilon = 0.05$, $\delta = 4$ and $\kappa = 2\pi/3$,[3] the average residual squares at different orders of approximation are shown in Fig. 2. Fig. 2 shows the convergence domain is $[-1.5, 0)$, that means we would obtain convergent high-order series solutions for any value of C_0 that satisfy $-1.5 \le C_0 < 0$. Strictly speaking, the optimal convergence-parameter should be obtained as the order tends to infinity. Fortunately, this is unnecessary: it is not our purpose to find out the exact value of the optimal convergence-control parameter, since an approximate value of it is good enough and can give fast enough convergence! Note for the residual of governing equation (15) ε_m^g, the optimal convergence-parameter changes a little at different orders of approximations. Here $C_0 = -0.8$ is considered and the residuals ε_m^g, $\varepsilon_m^{b,1}$ and $\varepsilon_m^{b,2}$ decrease quickly as the order of approximation m increases, as shown in Fig. 3. So in our model, the convergence-control parameter indeed provides us a convenient way to guarantee the convergence of series solutions. To increase the convergent rate of the series solution, the Homotopy–Pade approximation is applied and the corresponding $[m, m]$ approximation of c_1 and c_2 is shown in Table 2. Table 2 shows that as the approximation order n increases, the values of $[m, m]$ Homotopy–Pade approximation of c_1 and c_2 gradually tend to constants. Hereinafter all the following calculations stop until the results of Homotopy–Pade approximation agree to five significant figures.

In summary, in the frame of the HAM, the original complicated nonlinear partial differential equations are transferred into an infinite number of linear sub-problems, which are efficiently solved by means of the computer algebra system

[3] Here $\kappa = 2\pi/3$ is applied to avoid the influence of the resonant interaction: small divisors arise in (C.12) and (C.13) and this value is applied in the rest part of this paper, without loss of generality.

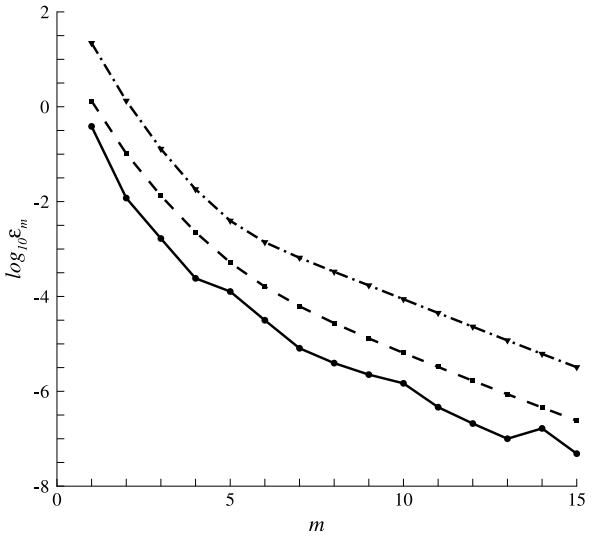

Fig. 3. $\log_{10}\varepsilon_m^g$, $\log_{10}\varepsilon_m^{b,1}$ and $\log_{10}\varepsilon_m^{b,2}$ versus the approximation order m with $H_1 = H_2 = 0.1$, $\varepsilon = 0.05$, $\delta = 4$, $\kappa = 2\pi/3$ and $C_0 = -0.8$. Solid line: $\log_{10}\varepsilon_m^g$; Dashed line: $\log_{10}\varepsilon_m^{b,1}$; Dash–dot line: $\log_{10}\varepsilon_m^{b,2}$.

Table 2
$[m, m]$ Homotopy–Pade approximation of c_1 and c_2 with $H_1 = H_2 = 0.1$, $\varepsilon = 0.05$, $\delta = 4$ and $\kappa = 2\pi/3$.

m	c_1	c_2
1	1.02524	1.05651
2	1.02509	1.06007
3	1.02529	1.06123
4	1.02557	1.05910
5	1.02558	1.05918
6	1.02558	1.05918
7	1.02558	1.05918

such as Mathematica. Especially, the convergence of series solutions is guaranteed by means of the so-called convergence-control parameter. In this way, we can gain the series approximations of the unidirectional bichromatic wave-train riding on exponentially sheared current.

4. Result analysis

First of all, we consider the phase velocity of the linear wave propagating over the exponentially sheared current. The changes of the phase velocity due to the surface velocity and the characteristic depth of the current is compared with previous work. As the amplitude of each primary wave increases, the nonlinear effect of the wave interaction needs to be considered. So, a high-order approximation of the phase velocity concerning both the self–self and mutual interactions of primary waves is established. Finally, we illustrate how the vorticity influences the phase velocity caused by the nonlinear wave mutual interaction in exponentially sheared current fields.

4.1. Linear wave propagating on exponentially sheared current

Linear wave is initially considered here to validate the solution procedure and to also serve as a benchmark for finite-amplitude waves. For the linear wave propagating over the weak current, the dispersion relation in water of infinite depth

$$c = 1 + \frac{2\varepsilon}{2+\delta} \tag{28}$$

is first derived by Stewart and Joy [7] and the extension to the second order

$$c = 1 + \frac{2\varepsilon}{2+\delta} + \frac{\varepsilon^2}{2(1+\delta)} - \frac{2\varepsilon^2}{(2+\delta)^2} \tag{29}$$

is given by Kirby and Chen [10]. It is shown by Skop [8] that the first-order approximation (28) provides generally good estimates of the wave parameters, while Kirby and Chen [10] remarked that there is a general overall deviation between the

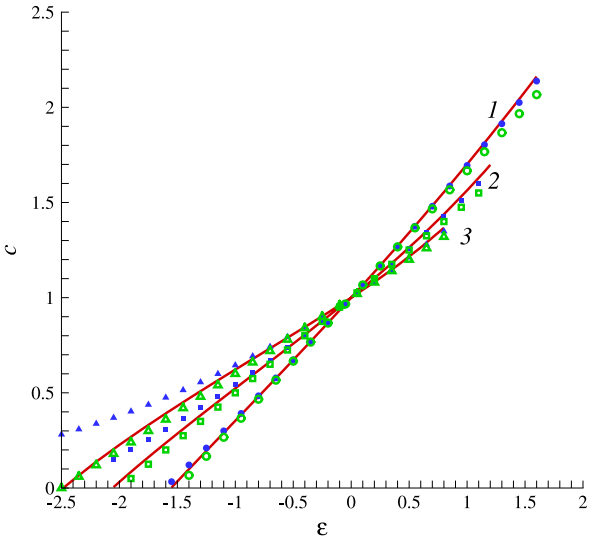

Fig. 4. (Color online) Phase velocity c versus current strength ε when $H = 0.001$. Open points correspond to (28) and filled points correspond to (29). Curve labels are values of δ.

dispersion curves for the first (28) and second (29) approximations, which reflecting the reduced accuracy of the first-order approximation (28).

Fig. 4 shows phase velocity c versus surface velocity $\varepsilon = U_0/\sqrt{g/k}$ with a range of characteristic slope $\delta = 1/(kd)$ for amplitude $H = 0.001$. For currents with weak vorticity ($\varepsilon\delta < 1$), there is close agreement among the first-order (28), second-order (29) perturbation approximations and the high-order (C.16) HAM approximations. This consistency verifies the validity of our analytic approach based on the HAM. For the current with stronger vorticity ($\varepsilon\delta > 1$), there is a deviation of c between the first-order (28) and second-order (29) approximations, especially for the strong opposing current. And it is a surprise to find that the high-order HAM approximations (C.16) agree well with the first-order perturbation approximation (28) over the whole region of ε, mainly because the corresponding nonlinearity is weak. The deviation with the second-order approximations [10] for the current with strong vorticity needs further investigation, especially by experiments.

As δ increases, the phase speed decreases for following currents $\varepsilon > 0$ but increases for opposing currents $\varepsilon < 0$, as shown in Fig. 4. So, for linear waves, the characteristic slope δ always act to reduce the change of phase velocity caused by surface current strength ε. In other words, the mean flow vorticity $\varepsilon\delta$ tends to reduce the effect of the surface current velocity ε on the linear phase velocity. This result is consistent with Swan and James [18] who concluded that for the weak current case the vorticity distribution acts to reduce the effective Doppler shift.

4.2. Interaction of two finite-amplitude waves without current

When the amplitudes of each primary wave increase, the nonlinear interaction affects the phase velocity, greatly. For finite-amplitude waves without currents, the dispersion relation of jth primary waves reduces to

$$c_j = 1 + c_j^S(H_j) + c_j^I(\kappa, H_1, H_2), \quad j = 1, 2. \tag{30}$$

For two primary waves traveling in the same direction, we consider $H_1 = H_2 = H$ for simplicity so that $c_1^S = c_2^S$, but $c_1^I \neq c_2^I$ since $\kappa \neq 1$. It is found that, when $H \leq 0.1$, the values of c_j^I agree well with that in the third-order perturbation theory of Longuet-Higgins and Phillips [30],[4] as shown in Fig. 5. In fact, the coefficients of the leading terms in c_j^I given by the HAM is the same as those in [30]: this explains the well agreement for small-amplitude waves. This consistency verifies the validity of our analytic approach based on the HAM for finite-amplitude waves without current.

As the amplitude H increases, the mutual nonlinear interaction between each primary component becomes stronger, which means the increase of c_j^I for primary waves traveling along each other. Fig. 5 shows the value of c_j^I do increase as H increases, and those values are always bigger than that given by the third-order perturbation theory [30], especially for c_2^I (the phase-velocity of the shorter wave caused by the longer ones). For a bigger value of H, the deviation becomes more remarkable, which indicates clearly the important role of the high-order approximations for finite-amplitude wave interactions. The $[m, n]$ Homotopy–Pade approximation of c_j^I at $H = 0.14$ is shown in Table 3, which illustrates the convergence of the high-order approximations together with the difference between low-order and high-order approximations in HAM.

[4] A misprint in equation (2.8) was noted later, see Hogan et al. [31].

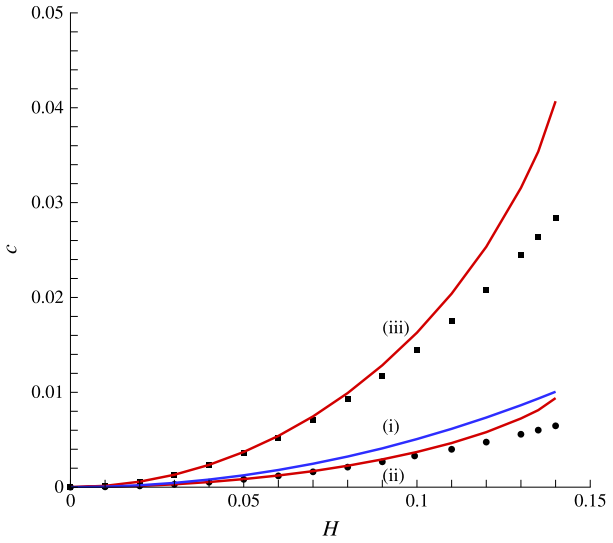

Fig. 5. (Color online) Phase velocity caused by self–self interaction c^S and mutual interactions c_1^I and c_2^I as a function of equivalent increasing stream function amplitude $H_1 = H_2 = H$ when $\kappa = 2\pi/3$ and the two primary waves moving in the same direction. (i) c^S; (ii) c_1^I; (iii) c_2^I. Points correspond to third-order theory [30]: •, c_1^I; ■, c_2^I.

Table 3
$[m, m]$ Homotopy–Pade approximation of c_1^I and c_2^I with $H = 0.14$ and $\kappa = 2\pi/3$.

m	c_1^I	c_2^I
1	0.0081	0.0307
5	0.0089	0.0392
9	0.0094	0.0420
13	0.0094	0.0407
15	0.0094	0.0407

Table 4
[15, 15] Homotopy–Pade approximation of coefficients for $H_1 = H_2 = 0.14$, $\kappa = 2\pi/3$.

Surface elevation		Stream function	
$C^{\zeta}_{1,0}$	0.14079	$C^{\psi}_{1,0}$	0.43849
$C^{\zeta}_{0,1}$	0.06735	$C^{\psi}_{0,1}$	0.14467
$C^{\zeta}_{2,0}$	0.01124	$C^{\psi}_{2,0}$	0.00278
$C^{\zeta}_{1,1}$	0.01665	$C^{\psi}_{1,1}$	0.00313
$C^{\zeta}_{1,-1}$	−0.00714	$C^{\psi}_{1,-1}$	−0.05331
$C^{\zeta}_{0,2}$	0.01021	$C^{\psi}_{0,2}$	0.00186

On the whole range of $0 \le H \le 0.14$, c_2^I is larger than c^S that is larger than c_1^I. Apparently, the longer waves have a greater influence on the shorter waves then vice versa. When $H = 0.14$, the ratio c_2^I over c^S reaches 4.04, while $c_1^I/c^S \approx 0.93$. It suggests that, as the amplitudes of primary waves increase, the phase velocity of the shorter wave caused by the longer one deserves more attention than other components of the phase velocity. So, as a representative of the phase velocity caused by the nonlinear wave interaction only c_2^I (the phase velocity related to the mutual interaction of the shorter wave) is considered in the rest part of this paper. For $H_1 = H_2 = 0.14$, the [10, 10] and [15, 15] Homotopy–Pade approximations of the surface elevations are shown in Fig. 6. The overlap of surface elevation between different orders shows the convergence of the solution. And the relevant coefficients $C^{\zeta}_{i,j}$ and $C^{\phi}_{i,j}$ related to Fig. 6 are given in Table 4 for $|i| + |j| <= 2$ for further comparison with experimental or numerical results.

In many practical wave fields, the primary waves may travel against each other. Table 5 shows the values of c_2^I for a shorter wave that traveling both along and against the longer ones. When the amplitude is small ($H = 0.02$), the magnitude of c_2^I is the same in two cases. The conclusion of [30] that the phase velocities are increased/decreased by the same amount as the propagation directions are the same/opposed stands at this case. For $H \ge 0.04$, the magnitude of c_2^I is always bigger when the two primary waves move in the same direction than that in the opposed direction. As the amplitude increases, the difference becomes more remarkable. So, for the interaction of finite-amplitude waves, high-order approximation is necessary so as to get more accurate predictions.

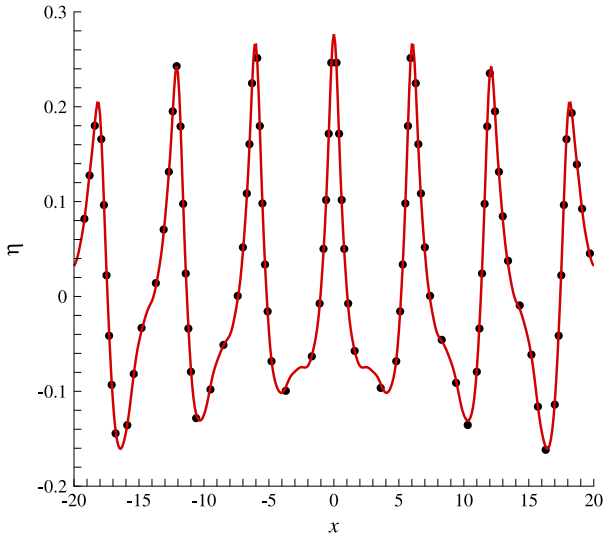

Fig. 6. (Color online) Surface elevation: [10, 10] Homotopy–Pade approximation (dot); [15, 15] Homotopy–Pade approximation (full line). Specifications: $H_1 = H_2 = 0.14, \kappa = 2\pi/3$.

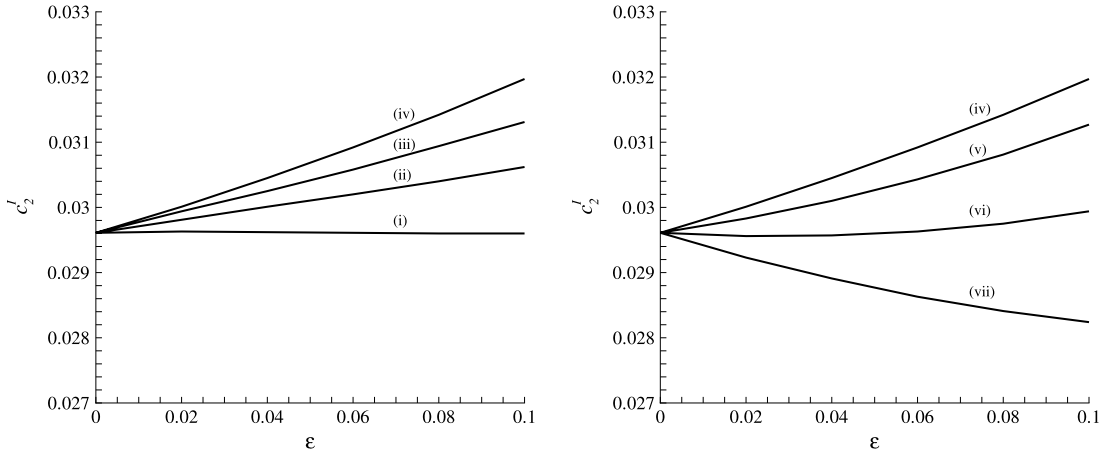

(a) Under critical slope δ_c. (b) Above critical slope δ_c.

Fig. 7. The effect of surface current strength ε on the phase velocity of the shorter wave caused by the longer one c_2^I. (i) $\delta = 0$; (ii) $\delta = 0.375$; (iii) $\delta = 0.75$; (iv) $\delta = 1.5$; (v) $\delta = 3$; (vi) $\delta = 4$; (vii) $\delta = 5$. Specifications: $H_1 = 0.14, H_2 = 0.02, \kappa = 2\pi/3$.

Table 5
Comparison of c_2^I between the shorter wave traveling along and against the longer wave. Specifications: $H_1 = H_2 = H, \kappa = 2\pi/3$.

H	0.02	0.04	0.06	0.08	0.10	0.12	0.13	0.14
Traveling along	0.0006	0.0024	0.0054	0.0099	0.0163	0.0253	0.0316	0.0407
Traveling against	0.0006	0.0023	0.0052	0.0093	0.0146	0.0210	0.0247	0.0287

4.3. Interaction of two finite-amplitude waves on exponentially sheared current

For finite-amplitude waves propagating on the exponentially sheared current, the nonlinear wave interactions are influenced by the current. As found in Section 4.2, the phase velocity of the shorter wave caused by the longer one acts as the leading role among the phase velocity caused by nonlinear wave interactions, so only the influence of vorticity on the phase velocity of the shorter wave caused by longer one c_2^I is considered. For simplicity, the amplitudes of the primary waves $H_1 = 0.14$ and $H_2 = 0.02$ are applied and both the primary waves and the exponentially sheared current are moving in the same direction. Both the effects of surface current velocity ε and characteristic slope δ on c_2^I are to be investigated.

The values of c_2^I for seven groups of characteristic slope $\delta = 0, 0.375, 0.75, 1.5, 3, 4, 5$ when the surface current velocity ε increases are shown in Fig. 7. Note that when $\delta = 0$ (corresponds to uniform current), $c_2^I \equiv 0.0296$ means only the

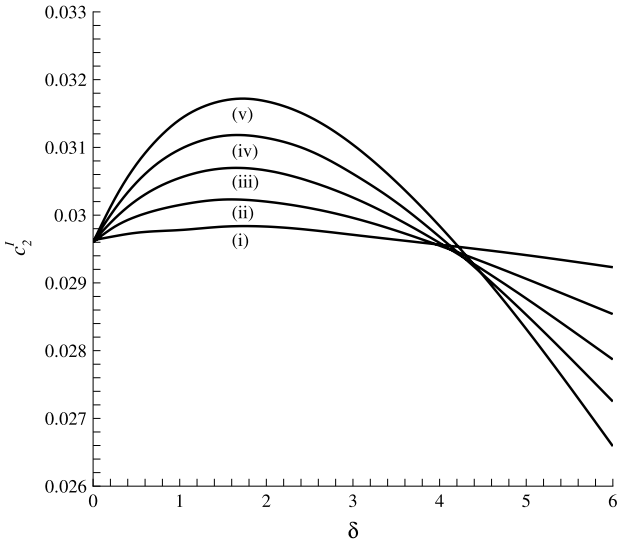

Fig. 8. The effect of the current characteristic slope δ on the phase velocity of the shorter wave caused by the longer one c_2^I. (i) $\varepsilon = 0.01$; (ii) $\varepsilon = 0.03$; (iii) $\varepsilon = 0.05$; (iv) $\varepsilon = 0.07$; (v) $\varepsilon = 0.09$. Specifications: $H_1 = 0.14, H_2 = 0.02, \kappa = 2\pi/3$.

non-uniform current affects c_2^I (nonlinear wave interactions). For any given surface current velocity $0 \leq \varepsilon \leq 0.1$, the increase of δ from 0 to 1.5 leads to an increase of c_2^I, as shown in Fig. 7(a), while the continued increase of δ from 1.5 to 5 leads to a decrease of c_2^I, as shown in Fig. 7(b), respectively. Thus, there exists a critical characteristic slope (near $\delta_c = 1.5$), under/above which the mean flow vorticity $\varepsilon\delta$ leads to the increase/decrease of c_2^I. Note that this tendency is more striking for larger values of ε (stronger currents).

The property of this critical characteristic slope δ_c can also be shown in Fig. 8 for five groups of ε. As the mean flow vorticity $\varepsilon\ \delta$ increases, the value of c_2^I increases in the range $0 \leq \delta \leq \delta_c$, with $\delta_c = 1.73$ determined from the case $\varepsilon = 0.09$. After it reaches the maximum value at the critical characteristic slope, it decreases with continuous increase of δ. Again this phenomenon is more remarkable for a bigger value of surface current velocity ε. Only when $\delta < 4$ the increase of ε will lead c_2^I to increase as compared to the pure bichromatic wave-train case, otherwise c_2^I decreases as ε increases.

More results show this critical characteristic slope δ_c appears in all components of the phase velocity caused by wave self–self and mutual wave interactions, each with a different critical value. If the bichromatic wave-train and the current are propagating opposed to each other, the critical characteristic slope δ_c still exists, under/above which the mean flow vorticity $\varepsilon\delta$ leads to the decrease/increase of the corresponding part of the phase velocity. Recalling the phase velocity of the small-amplitude wave shown in Fig. 4, we find that the phase velocity caused by nonlinear wave self–self and mutual interactions has a deeper reliance on the characteristic slope than the phase velocity of the linear wave. It is the current profile slope that determines the effect of vorticity on the nonlinear wave interaction, meanwhile the surface current strength may amplify/reduce this effect.

5. Conclusion

In this paper, the interaction between the unidirectional bichromatic wave-train and exponentially sheared current on infinite depth is investigated. Different from previous results, we do not make any assumptions on the wave amplitude. Besides, a current profile of the exponential type vertically is applied. So, both the effects of nonlinearity and vorticity are revealed for the interaction of the irregular wave and the current in this model.

This nonlinear partial differential equation is solved analytically by means of the HAM. Unlike perturbation methods which are based on small physical parameters, the HAM is independent of any small physical parameters at all. So, it enables us to obtain high-order approximations for finite-amplitude bichromatic waves. The convergence of solutions provided by HAM is guaranteed by the so-called convergence-control parameter. So theoretically speaking, these high-order approximations are effective and the HAM is valid for highly nonlinear problems, as illustrated by many examples mentioned by Liao [34,35]. Meanwhile, we acknowledge the accuracy of high-order approximations provided by HAM needs further comparison with experimental data.

Based on the convergent series solution gained by the HAM, some interesting conclusions are gained. First, the phase velocity of a small-amplitude wave traveled on exponentially sheared current is investigated without restriction on the surface velocity or the characteristic slope of the current. For current with weak vorticity, our series solutions are consistent with both the first-order [8] and second-order [10] dispersion relations provided by the perturbation method. For the current with stronger vorticity, there is a deviation between the first-order and second-order perturbation approximations, especially for the strong opposing current, but our high-order HAM approximations agree well with the first-order perturbation

approximations. Further investigation is needed to explain this discrepancy, especially by an experimental way. Besides, for small-amplitude waves it is found that the mean flow vorticity always acts to reduce the effect of the surface current velocity on the phase velocity.

Secondly, the phase velocity of the finite-amplitude unidirectional bichromatic wave-train without current is investigated. A high-order approximation of the phase velocity concerning both the self–self and mutual interactions of primary waves is established. It is found that, when the amplitudes of primary waves are small, the third-order perturbation theory [30] gives reliable prediction of the phase velocity caused by the mutual interaction. For the interaction of finite-amplitude waves, high-order approximations of the phase velocity is obtained for the first time. It is found that, as the amplitudes of the primary waves increase, the magnitude of the phase velocity of the shorter wave caused by the longer one is much bigger than other components of the phase velocity. In addition, the magnitude of the phase velocity caused by the mutual interaction owns a bigger value for primary waves moving in the same direction than those in opposed ones.

Thirdly, we investigated the effect of vorticity on the phase velocity caused by the nonlinear wave interaction in exponentially sheared current. The effect of vorticity on the phase velocity caused by the nonlinear wave interaction is different from that by linear ones. For each part of the phase velocity caused by wave self–self or mutual interactions, a critical characteristic current slope is found, under/above which the mean flow vorticity increases/reduces the corresponding part of the phase velocity. This tendency becomes more striking for big values of the current surface velocity. Thus, qualitatively speaking, the effect of vorticity on the phase velocity caused by nonlinear wave interactions is determined by the current profile slope, and this effect is amplified/reduced by the surface current strength.

We acknowledge that due to the constant exponential type current profile, no feedback from the current to the wave fields has been considered. This limitation restricts our calculations to the relative weak interaction between waves and currents. Note that the model considered in this work is rather general and investigating the feedback from the current to the wave fields in this model is one of our future works. Besides, triad resonant interactions may exist for irregular waves traveling on currents, which deserve our attention too. Certainly, it is an interesting and challenging work to study wave–current interactions when the primary waves propagate in arbitrary directions and ride on an ambient rotational current.

Acknowledgments

We would like to express our sincere acknowledgments to Prof. Per A. Madsen and Prof. Roger Grimshaw for their valuable suggestions during the course of the research. Thanks to the anonymous referees for their valuable comments and discussions. This work is partly supported by the National Natural Science Foundation of China (Approval No. 11272209), the State Key Laboratory of Ocean Engineering (Approval No. GKZD010061), and the Lloyd's Register Foundation (LRF). LRF invests in science, engineering and technology for public benefit, worldwide.

Appendix A. General form of deformation equations

Let $\psi_0(\xi_1, \xi_2, y)$, $\zeta_0(\xi_1, \xi_2)$, $c_{1,0}$, $c_{2,0}$ denote the initial guesses of ψ, ζ, c_1, c_2, respectively. According to the solution expressions (11) and (22), we choose

$$\zeta_0(\xi_1, \xi_2) = 0, \tag{A.1}$$

$$\psi_0(\xi_1, \xi_2, y) = C^{\psi}_{1,0,1,0,0}\cos(\xi_1)\exp(k_1 y) + C^{\psi}_{0,1,0,1,0}\cos(\xi_2)\exp(k_2 y) + U_0 d\exp(y/d) \tag{A.2}$$

as the initial guess of $\zeta(\xi_1, \xi_2)$ and $\psi(\xi_1, \xi_2, y)$, respectively. Here $C^{\psi}_{1,0,1,0,0}$ and $C^{\psi}_{0,1,0,1,0}$ are the coefficients of the terms $\cos(\xi_1)\exp(k_1 y)$, $\cos(\xi_2)\exp(k_2 y)$ in $\psi(\xi_1, \xi_2, y)$ so that these two terms do not appear in $\psi_m(\xi_1, \xi_2, y)$, $m \geq 1$, any more. The reason for this choice of $C^{\psi}_{1,0,1,0,0}$ and $C^{\psi}_{0,1,0,1,0}$ will be further explained in Appendix C.

Define a family of functions $\Psi(\xi_1, \xi_2, y; q)$, $\eta(\xi_1, \xi_2; q)$, $\lambda_1(q)$, $\lambda_2(q)$, where $q \in [0, 1]$ is called the embedding parameter. In HAM, these functions are governed by the so-called zeroth-order deformation equation

$$(1-q)\mathcal{L}_g[\Psi(\xi_1, \xi_2, y; q) - \psi_0(\xi_1, \xi_2, y), \lambda_1(q), \lambda_2(q)] = q\, C_0\, \mathcal{N}_g[\Psi(\xi_1, \xi_2, y; q), \lambda_1(q), \lambda_2(q)], \tag{A.3}$$

subject to the two boundary conditions

$$\begin{aligned}&(1-q)\mathcal{L}_{b,1}[\eta(\xi_1, \xi_2; q) - \zeta_0(\xi_1, \xi_2), \Psi(\xi_1, \xi_2, y; q) - \psi_0(\xi_1, \xi_2, y), \lambda_1(q), \lambda_2(q)]\\ &\quad = qC_0\mathcal{N}_{b,1}[\eta(\xi_1, \xi_2; q), \Psi(\xi_1, \xi_2, y; q), \lambda_1(q), \lambda_2(q)], \quad \text{on } y = \eta(\xi_1, \xi_2; q),\end{aligned} \tag{A.4}$$

$$\begin{aligned}&(1-q)\mathcal{L}_{b,2}[\eta(\xi_1, \xi_2; q) - \zeta_0(\xi_1, \xi_2), \Psi(\xi_1, \xi_2, y; q) - \psi_0(\xi_1, \xi_2, y), \lambda_1(q), \lambda_2(q)]\\ &\quad = qC_0\mathcal{N}_{b,2}[\eta(\xi_1, \xi_2; q), \Psi(\xi_1, \xi_2, y; q), \lambda_1(q), \lambda_2(q)] \quad \text{on } y = \eta(\xi_1, \xi_2; q),\end{aligned} \tag{A.5}$$

and the bed condition

$$k_1\frac{\partial\Psi(\xi_1, \xi_2, y; q)}{\partial\xi_1} + k_2\frac{\partial\Psi(\xi_1, \xi_2, y; q)}{\partial\xi_2} \to 0, \quad y \to -\infty, \tag{A.6}$$

where $q \in [0, 1]$ denotes the embedding parameter, C_0 is the convergence-control parameter, and the auxiliary linear operators $\mathcal{L}_g$, $\mathcal{L}_{b,1}$ and $\mathcal{L}_{b,2}$ are defined from (15) to (17).

Assuming that the convergence-control parameter C_0 is properly chosen so that the Taylor series expansions

$$\eta(\xi_1, \xi_2; q) = \sum_{m=0}^{+\infty} \zeta_m(\xi_1, \xi_2)\, q^m, \tag{A.7}$$

$$\Psi(\xi_1, \xi_2, y; q) = \sum_{m=0}^{+\infty} \psi_m(\xi_1, \xi_2, y)\, q^m, \tag{A.8}$$

$$\lambda_1(q) = \sum_{m=0}^{+\infty} c_{1,m}\, q^m, \tag{A.9}$$

$$\lambda_2(q) = \sum_{m=0}^{+\infty} c_{2,m}\, q^m, \tag{A.10}$$

exist and converge at $q = 1$, we have the so-called homotopy-series solution

$$\zeta(\xi_1, \xi_2) = \sum_{m=1}^{+\infty} \zeta_m(\xi_1, \xi_2), \tag{A.11}$$

$$\psi(\xi_1, \xi_2, y) = \psi_0(\xi_1, \xi_2, y) + \sum_{m=1}^{+\infty} \psi_m(\xi_1, \xi_2, y), \tag{A.12}$$

$$c_1 = c_{1,0} + \sum_{m=1}^{+\infty} c_{1,m}, \tag{A.13}$$

$$c_2 = c_{2,0} + \sum_{m=1}^{+\infty} c_{2,m}, \tag{A.14}$$

respectively.

The so-called mth-order deformation equations ($m \geq 1$) about $\zeta_m(\xi_1, \xi_2)$, $\psi_m(\xi_1, \xi_2, y)$, $c_{1,m}$ and $c_{2,m}$ in (A.11)–(A.14) can be derived directly from the zeroth-order deformation equations (A.3)–(A.6). For simplicity, we define the vectors

$$\boldsymbol{\zeta}_n = \{\zeta_0, \zeta_1, \zeta_2, \ldots, \zeta_n\}, \qquad \boldsymbol{\psi}_n = \{\psi_0, \psi_1, \psi_2, \ldots, \psi_n\},$$
$$\boldsymbol{c}_{1,n} = \{c_{1,0}, c_{1,1}, c_{1,2}, \ldots, c_{1,n}\}, \qquad \boldsymbol{c}_{2,n} = \{c_{2,0}, c_{2,1}, c_{2,2}, \ldots, c_{2,n}\}.$$

Substituting the Taylor series (A.7)–(A.10) into the zeroth-order deformation equations (A.3)–(A.6) with $y = \eta(\xi_1, \xi_2; q)$ for the two free-surface conditions, then equating the like-power of q, we have the mth-order deformation equations

$$\bar{\mathcal{L}}_g[\psi_m] = R_m^g(\boldsymbol{\psi}_{m-1}, \boldsymbol{c}_{1,m-1}, \boldsymbol{c}_{2,m-1}), \tag{A.15}$$

subject to the two free-surface boundary conditions on $y = 0$:

$$k_1 c_{1,0} \frac{\partial \zeta_m}{\partial \xi_1} + k_2 c_{2,0} \frac{\partial \zeta_m}{\partial \xi_2} - k_1 \frac{\partial \psi_m}{\partial \xi_1} - k_2 \frac{\partial \psi_m}{\partial \xi_2} = R_m^{b,1}(\boldsymbol{\zeta}_{m-1}, \boldsymbol{\psi}_{m-1}, \boldsymbol{c}_{1,m-1}, \boldsymbol{c}_{2,m-1}), \tag{A.16}$$

$$k_1 c_{1,0} \frac{\partial^2 \psi_m}{\partial \xi_1 \partial y} + k_2 c_{2,0} \frac{\partial^2 \psi_m}{\partial \xi_2 \partial y} - g k_1 \frac{\partial \zeta_m}{\partial \xi_1} - g k_2 \frac{\partial \zeta_m}{\partial \xi_2} = R_m^{b,2}(\boldsymbol{\zeta}_{m-1}, \boldsymbol{\psi}_{m-1}, \boldsymbol{c}_{1,m-1}, \boldsymbol{c}_{2,m-1}), \tag{A.17}$$

and the bed condition at infinity

$$k_1 \frac{\partial \psi_m}{\partial \xi_1} + k_2 \frac{\partial \psi_m}{\partial \xi_2} \to 0, \quad y \to -\infty. \tag{A.18}$$

The detailed deductions of the above higher-order deformation equations and the definitions of $\bar{\mathcal{L}}_g$, R_m^g, $R_m^{b,1}$ and $R_m^{b,2}$ are given in Appendix B. The solution procedure of $\zeta_m(\xi_1, \xi_2)$, $\psi_m(\xi_1, \xi_2, y)$, $c_{1,m}$ and $c_{2,m}$ are shown in Appendix C.

Appendix B. Detailed formulas in deformation equations

According to (A.8), we have

$$k_1^2 \frac{\partial^2 \Psi}{\partial \xi_1^2} + 2k_1 k_2 \frac{\partial^2 \Psi}{\partial \xi_1 \partial \xi_2} + k_2^2 \frac{\partial^2 \Psi}{\partial \xi_2^2} + \frac{\partial^2 \Psi}{\partial y^2} = \sum_{m=0}^{+\infty} \Pi_m(\xi_1, \xi_2, y) q^m, \tag{B.1}$$

where

$$\Pi_m(\xi_1, \xi_2, y) = k_1^2 \sum_{n=0}^{m} \frac{\partial \psi_n}{\partial \xi_1} \frac{\partial \psi_{m-n}}{\partial \xi_1} + 2k_1 k_2 \sum_{n=0}^{m} \frac{\partial \psi_n}{\partial \xi_1} \frac{\partial \psi_{m-n}}{\partial \xi_2} + k_2^2 \sum_{n=0}^{m} \frac{\partial \psi_n}{\partial \xi_2} \frac{\partial \psi_{m-n}}{\partial \xi_2} + \sum_{n=0}^{m} \frac{\partial \psi_n}{\partial y} \frac{\partial \psi_{m-n}}{\partial y}, \tag{B.2}$$

and similarly

$$\mathcal{N}_g[\Psi(\xi_1,\xi_2,y;q),\lambda_1(q),\lambda_2(q)]=\sum_{m=0}^{+\infty}\Delta_m^g q^m, \tag{B.3}$$

where

$$\Delta_m^g=\sum_{n=0}^{m}\left(k_1\frac{\partial\Pi_n}{\partial\xi_1}c_{1,m-n}+k_2\frac{\partial\Pi_n}{\partial\xi_2}c_{2,m-n}\right)-\sum_{n=0}^{m}\frac{\partial\psi_n}{\partial y}\left(k_1\frac{\partial\Pi_{m-n}}{\partial\xi_1}+k_2\frac{\partial\Pi_{m-n}}{\partial\xi_2}\right)$$
$$+\sum_{n=0}^{m}\left(k_1\frac{\partial\psi_n}{\partial\xi_1}+k_2\frac{\partial\psi_n}{\partial\xi_2}\right)\frac{\partial\Pi_{m-n}}{\partial y}, \tag{B.4}$$

respectively. Write

$$\frac{\partial^{i+j}\Psi}{\partial\xi_1^i\partial\xi_2^j}=\sum_{n=0}^{+\infty}\bar{\psi}_n^{i,j}(\xi_1,\xi_2)q^n, \tag{B.5}$$

$$\frac{\partial^{i+j}}{\partial\xi_1^i\partial\xi_2^j}\frac{\partial\Psi}{\partial y}=\sum_{n=0}^{+\infty}\bar{\psi}_{y,n}^{i,j}(\xi_1,\xi_2)q^n, \tag{B.6}$$

$$\frac{\partial^{i+j}}{\partial\xi_1^i\partial\xi_2^j}\frac{\partial^2\Psi}{\partial y^2}=\sum_{n=0}^{+\infty}\bar{\psi}_{yy,n}^{i,j}(\xi_1,\xi_2)q^n, \tag{B.7}$$

where

$$\bar{\psi}_n^{i,j}(\xi_1,\xi_2)=\sum_{m=0}^{n}\beta_{i,j}^{n-m,m}, \tag{B.8}$$

$$\bar{\psi}_{y,n}^{i,j}(\xi_1,\xi_2)=\sum_{m=0}^{n}\gamma_{i,j}^{n-m,m}, \tag{B.9}$$

$$\bar{\psi}_{yy,n}^{i,j}(\xi_1,\xi_2)=\sum_{m=0}^{n}\delta_{i,j}^{n-m,m}, \tag{B.10}$$

and the definitions of $\beta_{i,j}^{n-m,m}$, $\gamma_{i,j}^{n-m,m}$ and $\delta_{i,j}^{n-m,m}$ are given by [40].

Then, on $y=\eta(\xi_1,\xi_2;q)$, it holds using (A.7), (A.9), (A.10), (B.5), (B.6) and (B.7) that

$$\frac{\partial\Psi}{\partial y}\left(k_1\frac{\partial\eta}{\partial\xi_1}+k_2\frac{\partial\eta}{\partial\xi_2}\right)=\sum_{m=0}^{+\infty}\bar{\psi}_{y,m}^{0,0}q^m\sum_{n=0}^{+\infty}\left(k_1\frac{d\zeta_n}{d\xi_1}+k_2\frac{d\zeta_n}{d\xi_2}\right)q^n=\sum_{m=0}^{+\infty}\Gamma_{m,0}q^m, \tag{B.11}$$

$$\frac{\partial\Psi}{\partial y}\left(k_1\frac{\partial^2\Psi}{\partial\xi_1\partial y}+k_2\frac{\partial^2\Psi}{\partial\xi_2\partial y}\right)=\sum_{m=0}^{+\infty}\bar{\psi}_{y,m}^{0,0}q^m\sum_{n=0}^{+\infty}\left(k_1\bar{\psi}_{y,n}^{1,0}+k_2\bar{\psi}_{y,n}^{0,1}\right)q^n=\sum_{m=0}^{+\infty}\Gamma_{m,1}q^m, \tag{B.12}$$

$$\left(k_1\frac{\partial\Psi}{\partial\xi_1}+k_2\frac{\partial\Psi}{\partial\xi_2}\right)\frac{\partial^2\Psi}{\partial y^2}=\sum_{m=0}^{+\infty}\left(k_1\bar{\psi}_m^{1,0}+k_2\bar{\psi}_m^{0,1}\right)q^m\sum_{n=0}^{+\infty}\bar{\psi}_{yy,n}^{0,0}q^n=\sum_{m=0}^{+\infty}\Gamma_{m,2}q^m, \tag{B.13}$$

$$\frac{\partial\Psi}{\partial y}\left(k_1^2\frac{\partial^2\Psi}{\partial{\xi_1}^2}+2k_1k_2\frac{\partial^2\Psi}{\partial\xi_1\partial\xi_2}+k_2^2\frac{\partial^2\Psi}{\partial{\xi_2}^2}\right)$$
$$=\sum_{m=0}^{+\infty}\bar{\psi}_{y,m}^{0,0}q^m\sum_{n=0}^{+\infty}\left(k_1^2\bar{\psi}_n^{2,0}+2k_1k_2\bar{\psi}_n^{1,1}+k_2^2\bar{\psi}_n^{0,2}\right)q^n=\sum_{m=0}^{+\infty}\Gamma_{m,3}q^m, \tag{B.14}$$

$$\left(k_1\frac{\partial\Psi}{\partial\xi_1}+k_2\frac{\partial\Psi}{\partial\xi_2}\right)\left(k_1\frac{\partial^2\Psi}{\partial\xi_1\partial y}+k_2\frac{\partial^2\Psi}{\partial\xi_2\partial y}\right)$$
$$=\sum_{m=0}^{+\infty}\left(k_1\bar{\psi}_m^{1,0}+k_2\bar{\psi}_m^{0,1}\right)q^m\sum_{n=0}^{+\infty}\left(k_1\bar{\psi}_{y,n}^{1,0}+k_2\bar{\psi}_{y,n}^{0,1}\right)q^n=\sum_{m=0}^{+\infty}\Gamma_{m,4}q^m, \tag{B.15}$$

$$k_1^2\lambda_1\frac{\partial^2\Psi}{\partial{\xi_1}^2}+(\lambda_1+\lambda_2)k_1k_2\frac{\partial^2\Psi}{\partial\xi_1\partial\xi_2}+k_2^2\lambda_2\frac{\partial^2\Psi}{\partial{\xi_2}^2}$$
$$=k_1^2\sum_{m=0}^{+\infty}c_{1,m}q^m\sum_{n=0}^{+\infty}\bar{\psi}_n^{2,0}q^n+k_1k_2\sum_{m=0}^{+\infty}\left(c_{1,m}+c_{2,m}\right)q^m\sum_{n=0}^{+\infty}\bar{\psi}_n^{1,1}q^n$$
$$+k_2^2\sum_{m=0}^{+\infty}c_{2,m}q^m\sum_{n=0}^{+\infty}\bar{\psi}_n^{0,2}q^n=\sum_{m=0}^{+\infty}\Gamma_{m,5}q^m, \tag{B.16}$$

where

$$\Gamma_{m,0}=\sum_{n=0}^{m}\left(k_1\frac{d\zeta_n}{d\xi_1}+k_2\frac{d\zeta_n}{d\xi_2}\right)\bar{\psi}_{y,m-n}^{0,0}, \tag{B.17}$$

$$\Gamma_{m,1}=\sum_{n=0}^{m}\left(k_1\bar{\psi}_{y,n}^{1,0}+k_2\bar{\psi}_{y,n}^{0,1}\right)\bar{\psi}_{y,m-n}^{0,0}, \tag{B.18}$$

$$\Gamma_{m,2}=\sum_{n=0}^{m}\bar{\psi}_{yy,n}^{0,0}\left(k_1\bar{\psi}_{m-n}^{1,0}+k_2\bar{\psi}_{m-n}^{0,1}\right), \tag{B.19}$$

$$\Gamma_{m,3}=\sum_{n=0}^{m}\left(k_1^2\bar{\psi}_n^{2,0}+2k_1k_2\bar{\psi}_n^{1,1}+k_2^2\bar{\psi}_n^{0,2}\right)\bar{\psi}_{y,m-n}^{0,0}, \tag{B.20}$$

$$\Gamma_{m,4}=\sum_{n=0}^{m}\left(k_1\bar{\psi}_{y,n}^{1,0}+k_2\bar{\psi}_{y,n}^{0,1}\right)\left(k_1\bar{\psi}_{m-n}^{1,0}+k_2\bar{\psi}_{m-n}^{0,1}\right), \tag{B.21}$$

$$\Gamma_{m,5}=k_1^2\sum_{n=0}^{m}\bar{\psi}_n^{2,0}c_{1,m-n}+k_1k_2\sum_{n=0}^{m}\bar{\psi}_n^{1,1}\left(c_{1,m-n}+c_{2,m-n}\right)+k_2^2\sum_{n=0}^{m}\bar{\psi}_n^{0,2}c_{2,m-n}. \tag{B.22}$$

Furthermore, using (A.7) and (B.14)–(B.16), we have

$$\left\{k_1^2\lambda_1\frac{\partial^2\Psi}{\partial{\xi_1}^2}+(\lambda_1+\lambda_2)k_1k_2\frac{\partial^2\Psi}{\partial\xi_1\partial\xi_2}+k_2^2\lambda_2\frac{\partial^2\Psi}{\partial{\xi_2}^2}-\frac{\partial\Psi}{\partial y}\left(k_1^2\frac{\partial^2\Psi}{\partial{\xi_1}^2}+2k_1k_2\frac{\partial^2\Psi}{\partial\xi_1\partial\xi_2}\right.\right.$$
$$\left.\left.+k_2^2\frac{\partial^2\Psi}{\partial{\xi_2}^2}\right)+\left(k_1\frac{\partial\Psi}{\partial\xi_1}+k_2\frac{\partial\Psi}{\partial\xi_2}\right)\left(k_1\frac{\partial^2\Psi}{\partial\xi_1\partial y}+k_2\frac{\partial^2\Psi}{\partial\xi_2\partial y}\right)+g\right\}\left(k_1\frac{\partial\eta}{\partial\xi_1}+k_2\frac{\partial\eta}{\partial\xi_2}\right)$$
$$=\sum_{m=0}^{+\infty}\left(\Gamma_{m,5}-\Gamma_{m,3}+\Gamma_{m,4}+g(1-\chi_{m+1})\right)q^m\sum_{n=0}^{+\infty}\left(k_1\frac{d\zeta_n}{d\xi_1}+k_2\frac{d\zeta_n}{d\xi_2}\right)q^n$$
$$=\sum_{m=0}^{+\infty}\Lambda_{m,1}q^m, \tag{B.23}$$

where

$$\Lambda_{m,1}=\sum_{n=0}^{m}\left(k_1\frac{d\zeta_n}{d\xi_1}+k_2\frac{d\zeta_n}{d\xi_2}\right)\left(\Gamma_{m-n,5}-\Gamma_{m-n,3}+\Gamma_{m-n,4}+g(1-\chi_{m-n+1})\right). \tag{B.24}$$

Then, using (A.7), (B.5), (B.6), (B.11)–(B.13), and (B.24), we have on $y=\eta(\xi_1,\xi_2;q)$ that

$$\mathcal{N}_{b,1}[\eta(\xi_1,\xi_2;q),\Psi(\xi_1,\xi_2,y;q),\lambda_1(q),\lambda_2(q)]=\sum_{m=0}^{+\infty}\Delta_m^{b,1}q^m, \tag{B.25}$$

$$\mathcal{N}_{b,2}[\eta(\xi_1,\xi_2;q),\Psi(\xi_1,\xi_2,y;q),\lambda_1(q),\lambda_2(q)]=\sum_{m=0}^{+\infty}\Delta_m^{b,2}q^m, \tag{B.26}$$

where

$$\Delta_m^{b,1}=k_1\sum_{n=0}^{m}\frac{\partial\zeta_n}{\partial\xi_1}c_{1,m-n}+k_2\sum_{n=0}^{m}\frac{\partial\zeta_n}{\partial\xi_2}c_{2,m-n}-\Gamma_{m,0}-k_1\bar{\psi}_m^{1,0}-k_2\bar{\psi}_m^{0,1}, \tag{B.27}$$

$$\Delta_m^{b,2}=k_1\sum_{n=0}^{m}\psi_{y,n}^{1,0}c_{1,m-n}+k_2\sum_{n=0}^{m}\psi_{y,n}^{0,1}c_{2,m-n}-\Gamma_{m,1}+\Gamma_{m,2}-\Lambda_{m,1}. \tag{B.28}$$

Using (A.8) and (A.9), we have

$$c_1\frac{\partial^3(\Psi-\psi_0)}{\partial\xi_1^3}=\sum_{m=0}^{+\infty}c_{1,m}q^m\sum_{n=1}^{+\infty}\frac{\partial^3\psi_n}{\partial\xi_1^3}q^n=\sum_{m=1}^{+\infty}\sum_{n=0}^{m-1}c_{1,n}\frac{\partial^3\psi_{m-n}}{\partial\xi_1^3}q^m. \tag{B.29}$$

Then, it holds due to the linear property of the operator (15) that

$$\mathcal{L}_g(\Psi-\psi_0,\lambda_1,\lambda_2)=\sum_{m=1}^{+\infty}G_mq^m, \tag{B.30}$$

where

$$\begin{aligned}G_m=\;&k_1^3\sum_{n=0}^{m-1}c_{1,n}\frac{\partial^3\psi_{m-n}}{\partial\xi_1^3}+k_1^2k_2\sum_{n=0}^{m-1}(2c_{1,n}+c_{2,n})\frac{\partial^3\psi_{m-n}}{\partial\xi_1^2\partial\xi_2}+k_1k_2^2\sum_{n=0}^{m-1}(2c_{2,n}+c_{1,n})\frac{\partial^3\psi_{m-n}}{\partial\xi_1\partial\xi_2^2}+k_2^3\sum_{n=0}^{m-1}c_{2,n}\frac{\partial^3\psi_{m-n}}{\partial\xi_2^3}\\&+k_1\sum_{n=0}^{m-1}c_{1,n}\frac{\partial^3\psi_{m-n}}{\partial\xi_1\partial y^2}+k_2\sum_{n=0}^{m-1}c_{2,n}\frac{\partial^3\psi_{m-n}}{\partial\xi_2\partial y^2}.\end{aligned} \tag{B.31}$$

Thus, the left-hand side of (A.3) can be reduced to

$$(1-q)\mathcal{L}_g(\Psi-\psi_0,\lambda_1,\lambda_2)=(1-q)\sum_{m=1}^{+\infty}G_mq^m=\sum_{m=1}^{+\infty}(G_m-\chi_mG_{m-1})q^m. \tag{B.32}$$

Substituting (B.32), (B.3) into (A.3) and equating the like-power of q, we have the mth-order deformation equation of the vorticity transport equation:

$$G_m-\chi_mG_{m-1}=C_0\Delta_{m-1}^g,\quad m\geq1 \tag{B.33}$$

where

$$\chi_m=\begin{cases}0, & m\leq1,\\ 1, & m>1.\end{cases} \tag{B.34}$$

Define

$$\begin{aligned}\bar{G}_m=\;&k_1^3\sum_{n=1}^{m-1}c_{1,n}\frac{\partial^3\psi_{m-n}}{\partial\xi_1^3}+k_1^2k_2\sum_{n=1}^{m-1}(2c_{1,n}+c_{2,n})\frac{\partial^3\psi_{m-n}}{\partial\xi_1^2\partial\xi_2}+k_1k_2^2\sum_{n=1}^{m-1}(2c_{2,n}+c_{1,n})\frac{\partial^3\psi_{m-n}}{\partial\xi_1\partial\xi_2^2}+k_2^3\sum_{n=1}^{m-1}c_{2,n}\frac{\partial^3\psi_{m-n}}{\partial\xi_2^3}\\&+k_1\sum_{n=1}^{m-1}c_{1,n}\frac{\partial^3\psi_{m-n}}{\partial\xi_1\partial y^2}+k_2\sum_{n=1}^{m-1}c_{2,n}\frac{\partial^3\psi_{m-n}}{\partial\xi_2\partial y^2},\end{aligned} \tag{B.35}$$

$$\begin{aligned}\bar{\mathcal{L}}_g[\psi_m]=\;&k_1^3c_{1,0}\frac{\partial^3\psi_m}{\partial\xi_1^3}+k_1^2k_2(2c_{1,0}+c_{2,0})\frac{\partial^3\psi_m}{\partial\xi_1^2\partial\xi_2}+k_1k_2^2(2c_{2,0}+c_{1,0})\frac{\partial^3\psi_m}{\partial\xi_1\partial\xi_2^2}\\&+k_2^3c_{2,0}\frac{\partial^3\psi_m}{\partial\xi_2^3}+k_1c_{1,0}\frac{\partial^3\psi_m}{\partial\xi_1\partial y^2}+k_2c_{2,0}\frac{\partial^3\psi_m}{\partial\xi_2\partial y^2}.\end{aligned} \tag{B.36}$$

Then, (B.33) can be reduced to

$$\bar{\mathcal{L}}_g[\psi_m]=C_0\;\Delta_{m-1}^g+\chi_mG_{m-1}-\bar{G}_m=R_m^g(\boldsymbol{\psi}_{n-1},\boldsymbol{c}_{1,n-1},\boldsymbol{c}_{2,n-1}),\quad m\geq1. \tag{B.37}$$

Using (A.8) and (B.5), we have on $y=\eta(\xi_1,\xi_2;q)$ that

$$\frac{\partial(\Psi-\psi_0)}{\partial\xi_1}=\sum_{m=1}^{+\infty}\frac{\partial\psi_m(\xi_1,\xi_2,\eta)}{\partial\xi_1}q^m=\sum_{m=1}^{+\infty}q^m\sum_{n=0}^{+\infty}\beta_{1,0}^{m,n}q^n=\sum_{m=1}^{+\infty}\sum_{n=0}^{m-1}\beta_{1,0}^{m-n,n}q^m. \tag{B.38}$$

Similarly, on $y=\eta(\xi_1,\xi_2;q)$, it holds due to the linear property of the operator (16) that

$$(1-q)\mathcal{L}_{b,1}(\Psi-\psi_0,\eta-\zeta_0)=\sum_{m=1}^{+\infty}(S_m-\chi_mS_{m-1})q^m, \tag{B.39}$$

where

$$S_m(\xi_1,\xi_2)=\sum_{n=1}^{m}\left(k_1\frac{\partial\zeta_n}{\partial\xi_1}c_{1,m-n}+k_2\frac{\partial\zeta_n}{\partial\xi_2}c_{2,m-n}\right)-\sum_{n=0}^{m-1}\left(k_1\beta_{1,0}^{m-n,n}+k_2\beta_{0,1}^{m-n,n}\right). \tag{B.40}$$

Substituting (B.39), (B.25) into (A.4) and equating the like-power of q, we have the mth-order deformation equation for the kinematic free surface boundary condition:

$$S_m(\xi_1,\xi_2)-\chi_mS_{m-1}(\xi_1,\xi_2)=C_0\;\Delta_{m-1}^{b,1}(\xi_1,\xi_2),\quad m\geq1. \tag{B.41}$$

Introducing

$$\bar{S}_m(\xi_1,\xi_2)=\sum_{n=1}^{m-1}\left(k_1\frac{\partial\zeta_n}{\partial\xi_1}c_{1,m-n}+k_2\frac{\partial\zeta_n}{\partial\xi_2}c_{2,m-n}\right)-\sum_{n=1}^{m-1}\left(k_1\beta_{1,0}^{m-n,n}+k_2\beta_{0,1}^{m-n,n}\right), \tag{B.42}$$

we have

$$\begin{aligned}S_m &= k_1c_{1,0}\frac{\partial\zeta_m}{\partial\xi_1}+k_2c_{2,0}\frac{\partial\zeta_m}{\partial\xi_2}-k_1\beta_{1,0}^{m,0}-k_2\beta_{0,1}^{m,0}+\bar{S}_m\\ &= k_1c_{1,0}\frac{\partial\zeta_m}{\partial\xi_1}+k_2c_{2,0}\frac{\partial\zeta_m}{\partial\xi_2}-\left(k_1\frac{\partial\psi_m}{\partial\xi_1}+k_2\frac{\partial\psi_m}{\partial\xi_2}\right)\Big|_{y=0}+\bar{S}_m,\end{aligned} \tag{B.43}$$

and the following mth-order deformation equation on $y=0$:

$$\begin{aligned}&k_1c_{1,0}\frac{\partial\zeta_m}{\partial\xi_1}+k_2c_{2,0}\frac{\partial\zeta_m}{\partial\xi_2}-k_1\frac{\partial\psi_m}{\partial\xi_1}-k_2\frac{\partial\psi_m}{\partial\xi_2}\\ &\quad=C_0\,\Delta_{m-1}^{b,1}+\chi_mS_{m-1}-\bar{S}_m=R_m^{b,1}(\boldsymbol{\zeta}_{n-1},\boldsymbol{\psi}_{n-1},\boldsymbol{c}_{1,n-1},\boldsymbol{c}_{2,n-1}),\quad m\geq1.\end{aligned} \tag{B.44}$$

Similarly, the mth-order deformation equation for the dynamic surface boundary condition (on $y=0$) can be written as:

$$\begin{aligned}&k_1c_{1,0}\frac{\partial^2\psi_m}{\partial\xi_1\partial y}+k_2c_{2,0}\frac{\partial^2\psi_m}{\partial\xi_2\partial y}-gk_1\frac{\partial\zeta_m}{\partial\xi_1}-gk_2\frac{\partial\zeta_m}{\partial\xi_2}\\ &\quad=C_0\,\Delta_{m-1}^{b,2}+\chi_mT_{m-1}-\bar{T}_m=R_m^{b,2}(\boldsymbol{\zeta}_{n-1},\boldsymbol{\psi}_{n-1},\boldsymbol{c}_{1,n-1},\boldsymbol{c}_{2,n-1}),\quad m\geq1,\end{aligned} \tag{B.45}$$

where

$$\begin{aligned}T_m &= k_1c_{1,0}\gamma_{1,0}^{m,0}+k_2c_{2,0}\gamma_{0,1}^{m,0}-gk_1\frac{\partial\zeta_m}{\partial\xi_1}-gk_2\frac{\partial\zeta_m}{\partial\xi_2}+\bar{T}_m\\ &= k_1c_{1,0}\frac{\partial^2\psi_m}{\partial\xi_1\partial y}+k_2c_{2,0}\frac{\partial^2\psi_m}{\partial\xi_2\partial y}-gk_1\frac{\partial\zeta_m}{\partial\xi_1}-gk_2\frac{\partial\zeta_m}{\partial\xi_2}+\bar{T}_m,\end{aligned} \tag{B.46}$$

$$\bar{T}_m = k_1\sum_{l=1}^{m-1}c_{1,l}\sum_{n=0}^{m-l-1}\gamma_{1,0}^{m-l-n,n}+k_1c_{1,0}\sum_{n=1}^{m-1}\gamma_{1,0}^{m-n,n}+k_2\sum_{l=1}^{m-1}c_{2,l}\sum_{n=0}^{m-l-1}\gamma_{0,1}^{m-l-n,n}+k_2c_{2,0}\sum_{n=1}^{m-1}\gamma_{0,1}^{m-n,n}. \tag{B.47}$$

Appendix C. High-order solution procedure

According to the definition (B.36) of the auxiliary linear operators $\bar{\mathcal{L}}_g$, it holds for any positive integers M and N that

$$\bar{\mathcal{L}}_g\left[\sum_{i=0}^{M}\sum_{j=-M}^{M}\widetilde{C}_{i,j}^{\psi,m}\cos(i\xi_1+j\xi_2)\exp(|ik_1+jk_2|y)\right]=0, \tag{C.1}$$

where $\widetilde{C}_{i,j}^{\psi,m}$ are constants. Thus, the general solution of the high-order deformation equation (A.15) reads

$$\psi_m(\xi_1,\xi_2,y)=\psi_m^*(\xi_1,\xi_2,y)+\sum_{i=0}^{M}\sum_{j=-M}^{M}\widetilde{C}_{i,j}^{\psi,m}\cos(i\xi_1+j\xi_2)\exp(|ik_1+jk_2|y), \tag{C.2}$$

where

$$\psi_m^*(\xi_1,\xi_2,y)=\bar{\mathcal{L}}_g^{-1}\left[R_m^g(\boldsymbol{\psi}_{m-1},\boldsymbol{c}_{1,m-1},\boldsymbol{c}_{2,m-1})\right] \tag{C.3}$$

is the special solution, and the inverse operator $\bar{\mathcal{L}}_g^{-1}$ is defined by

$$\bar{\mathcal{L}}_g^{-1}\left[\sin(i\xi_1+j\xi_2)\exp(ny)\right]=\frac{\cos(i\xi_1+j\xi_2)\exp(ny)}{(ik_1c_{1,0}+jk_2c_{2,0})((ik_1+jk_2)^2-n^2)}. \tag{C.4}$$

To determine the unknown integration coefficients $\widetilde{C}_{i,j}^{\psi,m}$, we substitute (C.2) into (A.16) and (A.17) and get the following equations on $y=0$:

$$\begin{aligned}&k_1c_{1,0}\frac{\partial\zeta_m}{\partial\xi_1}+k_2c_{2,0}\frac{\partial\zeta_m}{\partial\xi_2}+\sum_{i=0}^{M}\sum_{j=-M}^{M}(ik_1+jk_2)\widetilde{C}_{i,j}^{\psi,m}\sin(i\xi_1+j\xi_2)\\ &\quad=\left(k_1\frac{\partial\psi_m^*}{\partial\xi_1}+k_2\frac{\partial\psi_m^*}{\partial\xi_2}\right)\Big|_{y=0}+R_m^{b,1}(\boldsymbol{\zeta}_{m-1},\boldsymbol{\psi}_{m-1},\boldsymbol{c}_{1,m-1},\boldsymbol{c}_{2,m-1}),\end{aligned} \tag{C.5}$$

$$-|ik_1+jk_2|\sum_{i=0}^{M}\sum_{j=-M}^{M}(ik_1c_{1,0}+jk_2c_{2,0})\widetilde{C}_{i,j}^{\psi,m}\sin(i\xi_1+j\xi_2)-gk_1\frac{\partial\zeta_m}{\partial\xi_1}-gk_2\frac{\partial\zeta_m}{\partial\xi_2}$$
$$=\left(-k_1c_{1,0}\frac{\partial^2\psi_m^*}{\partial\xi_1\partial y}-k_2c_{2,0}\frac{\partial^2\psi_m^*}{\partial\xi_2\partial y}\right)\Bigg|_{y=0}+R_m^{b,2}(\boldsymbol{\zeta}_{m-1},\boldsymbol{\psi}_{m-1},\boldsymbol{c}_{1,m-1},\boldsymbol{c}_{2,m-1}). \tag{C.6}$$

It is found that the right-hand side of the above two equations can be expressed by

$$\left(k_1\frac{\partial\psi_m^*}{\partial\xi_1}+k_2\frac{\partial\psi_m^*}{\partial\xi_2}\right)\Bigg|_{y=0}+R_m^{b,1}(\boldsymbol{\zeta}_{m-1},\boldsymbol{\psi}_{m-1},\boldsymbol{c}_{1,m-1},\boldsymbol{c}_{2,m-1})=\sum_{i=0}^{m}\sum_{j=-m}^{m}R_{i,j}^{1,m}(\boldsymbol{c}_{1,m-1},\boldsymbol{c}_{2,m-1})\sin(i\xi_1+j\xi_2), \tag{C.7}$$

$$\left(-k_1c_{1,0}\frac{\partial^2\psi_m^*}{\partial\xi_1\partial y}-k_2c_{2,0}\frac{\partial^2\psi_m^*}{\partial\xi_2\partial y}\right)\Bigg|_{y=0}+R_m^{b,2}(\boldsymbol{\zeta}_{m-1},\boldsymbol{\psi}_{m-1},\boldsymbol{c}_{1,m-1},\boldsymbol{c}_{2,m-1})$$
$$=\sum_{i=0}^{m}\sum_{j=-m}^{m}R_{i,j}^{2,m}(\boldsymbol{c}_{1,m-1},\boldsymbol{c}_{2,m-1})\sin(i\xi_1+j\xi_2), \tag{C.8}$$

where $R_{i,j}^{1,m}$ and $R_{i,j}^{2,m}$ are known coefficients. Balancing both sides of (C.5) and (C.6), we have $M=m$,

$$\zeta_m=\sum_{i=0}^{m}\sum_{j=-m}^{m}\widetilde{C}_{i,j}^{\zeta,m}\cos(i\xi_1+j\xi_2), \tag{C.9}$$

and the set of algebraic equations for the unknown $\widetilde{C}_{i,j}^{\zeta,m}$ and $\widetilde{C}_{i,j}^{\psi,m}$:

$$-(ik_1c_{1,0}+jk_2c_{2,0})\widetilde{C}_{i,j}^{\zeta,m}+(ik_1+jk_2)\widetilde{C}_{i,j}^{\psi,m}=R_{i,j}^{1,m}(\boldsymbol{c}_{1,m-1},\boldsymbol{c}_{2,m-1}), \tag{C.10}$$

$$-|ik_1+jk_2|(ik_1c_{1,0}+jk_2c_{2,0})\widetilde{C}_{i,j}^{\psi,m}+g(ik_1+jk_2)\widetilde{C}_{i,j}^{\zeta,m}=R_{i,j}^{2,m}(\boldsymbol{c}_{1,m-1},\boldsymbol{c}_{2,m-1}), \tag{C.11}$$

which has the solution

$$\widetilde{C}_{i,j}^{\zeta,m}=\frac{\left(ik_1c_{1,0}+jk_2c_{2,0}\right)R_{i,j}^{1,m}+sgn(ik_1+jk_2)R_{i,j}^{2,m}}{\left(g|ik_1+jk_2|-\left(ik_1c_{1,0}+jk_2c_{2,0}\right)^2\right)}, \tag{C.12}$$

$$\widetilde{C}_{i,j}^{\psi,m}=\frac{(ik_1+jk_2)\,gR_{i,j}^{1,m}+\left(ik_1c_{1,0}+jk_2c_{2,0}\right)R_{i,j}^{2,m}}{\left(g|ik_1+jk_2|-\left(ik_1c_{1,0}+jk_2c_{2,0}\right)^2\right)|ik_1+jk_2|}, \tag{C.13}$$

if $\left(g|ik_1+jk_2|-\left(ik_1c_{1,0}+jk_2c_{2,0}\right)^2\right)|ik_1+jk_2|\neq 0$. For $ij\neq 0$, the singularity caused by $g|ik_1+jk_2|-\left(ik_1c_{1,0}+jk_2c_{2,0}\right)^2=0$ is related to the resonant interaction and is considered beyond the scope of this paper. And the singularity caused by the appearance of $|ik_1+jk_2|=0$ in the dominator of $\widetilde{C}_{i,j}^{\psi,m}$ for the pure wave case may be removed since $R_{i,j}^{2,m}(\boldsymbol{c}_{1,m-1},\boldsymbol{c}_{2,m-1})$ intrinsically contains the term $|ik_1+jk_2|$. The last kind of singularity caused by $i=1,j=0$ and $i=0,j=1$ provides us equations to determine not only $\widetilde{C}_{1,0}^{\zeta,m}$, $\widetilde{C}_{1,0}^{\psi,m}$, $\widetilde{C}_{0,1}^{\zeta,m}$, $\widetilde{C}_{0,1}^{\psi,m}$ but also $c_{1,m-1}$ and $c_{2,m-1}$, as shown below in detail.

When $i=1,j=0$, Eqs. (C.10) and (C.11) reduce to

$$-k_1c_{1,0}\widetilde{C}_{1,0}^{\zeta,m}+k_1\widetilde{C}_{1,0}^{\psi,m}=R_{1,0}^{1,m}(\boldsymbol{c}_{1,m-1},\boldsymbol{c}_{2,m-1}), \tag{C.14}$$

$$-k_1^2c_{1,0}\widetilde{C}_{1,0}^{\psi,m}+gk_1\widetilde{C}_{1,0}^{\zeta,m}=R_{1,0}^{2,m}(\boldsymbol{c}_{1,m-1},\boldsymbol{c}_{2,m-1}). \tag{C.15}$$

Remembering the special choice of the initial guess solution (A.2), we declare that there should be no $\cos(\xi_1)\exp(k_1y)$, $\cos(\xi_2)\exp(k_2y)$ terms in (C.2), which means $\widetilde{C}_{1,0}^{\psi,m}=0$ in (C.14) and (C.15). So the remaining terms read

$$-k_1c_{1,0}\widetilde{C}_{1,0}^{\zeta,m}=R_{1,0}^{1,m}(\boldsymbol{c}_{1,m-1},\boldsymbol{c}_{2,m-1}),\qquad gk_1\widetilde{C}_{1,0}^{\zeta,m}=R_{1,0}^{2,m}(\boldsymbol{c}_{1,m-1},\boldsymbol{c}_{2,m-1}). \tag{C.16}$$

Apparently $\widetilde{C}_{1,0}^{\zeta,m}=R_{1,0}^{2,m}/(gk_1)$ and $R_{1,0}^{2,m}=-g/c_{1,0}R_{1,0}^{1,m}$ should be hold. It is from the last equation that we can get the value for $c_{1,m-1}$. For example, when $m=1$ the equation $R_{1,0}^{2,m}=-g/c_{1,0}R_{1,0}^{1,m}$ gives

$$(2dk_1^2+k_1)c_{1,0}^3-2dk_1^2U_0c_{1,0}^2-(2dgk_1+g)c_{1,0}+gU_0=0. \tag{C.17}$$

The solution of interest to this cubic equation is:

$$c_{1,0}=\begin{cases} B_1+\dfrac{2^{1/3}B_3}{3(2dk_1^2+k_1)\left(-B_2+\sqrt{B_2^2-4B_3^3}\right)^{1/3}}+\dfrac{2^{-1/3}\left(-B_2+\sqrt{B_2^2-4B_3^3}\right)^{1/3}}{3(2dk_1^2+k_1)} \\ B_1-\dfrac{2^{1/3}(1+\sqrt{3}i)B_3}{6(2dk_1^2+k_1)\left(-B_2+\sqrt{B_2^2-4B_3^3}\right)^{1/3}}-\dfrac{2^{-1/3}(1-\sqrt{3}i)\left(-B_2+\sqrt{B_2^2-4B_3^3}\right)^{1/3}}{6(2dk_1^2+k_1)} \end{cases} \tag{C.18}$$

where

$$B_1=\frac{2dk_1U_0}{3+6dk_1}, \tag{C.19}$$

$$B_2=9g(2dk_1-3)(1+2dk_1)^2k_1^2U_0-16d^3k_1^6U_0^3, \tag{C.20}$$

$$B_3=3g(1+2dk_1)^2k_1+4d^2k_1^4U_0^2. \tag{C.21}$$

The first solution in (C.18) denotes the phase velocity of a traveling wave propagating on following currents, which demands that the discriminant $\Delta=B_2^2-4B_3^3<0$. While the second one, related to waves traveling on opposing currents, is a real number all the time. In the case of no currents, the solution for $c_{1,0}$ coincides with the traditional linear phase speed $\pm\sqrt{g/k_1}$. In a similar way, $\widetilde{C}_{0,1}^{\zeta,m}$ and $c_{2,m-1}$ can be derived in the case of $i=0, j=1$. Thus, we gain the two unknown functions ψ_m, ζ_m and the two unknown constants $c_{1,m-1}$, $c_{2,m-1}$.

References

[1] P.D. Thompson, Ann. New York Acad. Sci. 51 (1949) 463–474.
[2] F. Biesel, Houille Blanche (1950) 279–285.
[3] O. Brink-Kjaer, Series Paper, 1976.
[4] J. Simmen, P. Saffman, Stud. Appl. Math. 75 (1985) 35–57.
[5] A. Teles da Silva, D. Peregrine, J. Fluid Mech. 195 (1988) 281–302.
[6] A.J. Abdullah, Ann. New York Acad. Sci. 51 (1949) 425–441.
[7] R. Stewart, J. Joy, Deep Sea Res. Oceanogr. Abstr. 21 (1974) 1039–1049.
[8] R.A. Skop, J. Waterway Port Coast. Ocean Eng. 113 (1987) 187–195.
[9] R.A. Skop, Appl. Math. Modelling 11 (1987) 432–437.
[10] J. Kirby, T. Chen, J. Geophys. Res. 94 (1989) 1013–1027.
[11] G. Thomas, J. Fluid Mech. 110 (1981) 457–474.
[12] R.A. Dalrymple, Water Wave Models and Wave Forces with Shear Currents, University of Florida, Coastal and Oceanographic Engineering Laboratory, 1973.
[13] R.A. Dalrymple, J. Geophys. Res. 79 (1974) 4498–4504.
[14] R. Dalrymple, J. Comput. Phys. 24 (1977) 29–42.
[15] G. Thomas, J. Fluid Mech. 216 (1990) 505–536.
[16] J. Ko, W. Strauss, J. Fluid Mech. 608 (2008) 197–215.
[17] J. Cheng, J. Cang, S. Liao, Z. Angew. Math. Phys. (ZAMP) 60 (2009) 450–478.
[18] C. Swan, R. James, Appl. Ocean Res. 22 (2000) 331–347.
[19] C. Swan, I. Cummins, R. James, J. Fluid Mech. 428 (2001) 273–304.
[20] D. Peregrine, Adv. Appl. Mech. 16 (1976) 9–117.
[21] D. Peregrine, I. Jonsson, Interaction of Waves and Currents, Technical Report, DTIC Document, 1983.
[22] G. Thomas, G. Klopman, Int. Ser. Adv. Fluid Mech. 10 (1997) 255–319.
[23] J. Lighthill, Waves in Fluids, Cambridge Univ. Pr., 2001.
[24] R. Simons, R. MacIver, Coastal Dynamics, ASCE, 2001, pp. 132–141.
[25] M. Umeyama, J. Waterway Port Coast. Ocean Eng. 135 (2009) 11–23.
[26] Q. Chen, P. Madsen, D. Basco, J. Waterway Port Coast. Ocean Eng. 125 (1999) 176–186.
[27] P. Madsen, D. Fuhrman, J. Fluid Mech. 557 (2006) 369–398.
[28] P. Madsen, D. Fuhrman, J. Fluid Mech. 698 (2012) 304–334.
[29] O. Nwogu, J. Fluid Mech. 627 (2009) 179–213.
[30] M. Longuet-Higgins, O. Phillips, J. Fluid Mech. 12 (1962) 333–336.
[31] S. Hogan, I. Gruman, M. Stiassnie, J. Fluid Mech. 192 (1988) 97–114.
[32] J. Zhang, L. Chen, J. Eng. Mech. 125 (1999) 768–779.
[33] M. Tanaka, C. Van, O. Oldrini, Phys. Fluids 14 (2002) 2109.
[34] S. Liao, Beyond Perturbation: Introduction to the Homotopy Analysis Method, CRC Press, 2003.
[35] S. Liao, Homotopy Analysis Method in Nonlinear Differential Equations, Springer & Higher Education Press, 2012.
[36] B.E. McDonald, J.M. Witting, J. Comput. Phys. 56 (1984) 237–243.
[37] V. Ekman, Ark. Mat. Astron. Fys. 2 (1905) 1–53.
[38] H. Xu, Z. Lin, S. Liao, J. Wu, J. Majdalani, Phys. Fluids 22 (2010) 053601.
[39] D. Xu, Z. Lin, S. Liao, M. Stiassnie, J. Fluid Mech. 710 (2012) 379–418.
[40] S. Liao, Commun. Nonlinear Sci. Numer. Simul. 16 (2011) 1274–1303.